ORNL/TM-12652

RECEIVED
JUL 15 1996
OSTI

ornl

OAK RIDGE NATIONAL LABORATORY

LOCKHEED MARTIN

The Calibration and Characterization of a Research X-Ray Unit

C. M. Johnson

MANAGED AND OPERATED BY
LOCKHEED MARTIN ENERGY RESEARCH CORPORATION
FOR THE UNITED STATES
DEPARTMENT OF ENERGY

ORNL-27 (3-96)

DISTRIBUTION OF THIS DOCUMENT IS UNLIMITED

MASTER

This report has been reproduced directly from the best available copy.

Available to DOE and DOE contractors from the Office of Scientific and Technical Information, P.O. Box 62, Oak Ridge, TN 37831; prices available from (615) 576-8401, FTS 626-8401.

Available to the public from the National Technical Information Service, U.S. Department of Commerce, 5285 Port Royal Rd., Springfield, VA 22161.

This report was prepared as an account of work sponsored by an agency of the United States Government. Neither the United States Government nor any agency thereof, nor any of their employees, makes any warranty, express or implied, or assumes any legal liability or responsibility for the accuracy, completeness, or usefulness of any informati9on, apparatus, product, or process disclosed, or represents that its use would not infringe privately owned rights. Reference herein to any specific commercial product, process, or service by trade name, trademark, manufacturer, or otherwise, does not necessarily constitute or imply its endorsement, recommendation, or favoring by the United States Government or any agency thereof. The views and opinions of authors expressed herein do not necessarily state or reflect those of the United States Government or any agency thereof.

ORNL/TM-12652

Health Sciences Research Division

The Calibration and Characterization of a Research X-Ray Unit

C. M. Johnson

Date Issued—June 1996

Prepared for
U.S. Department of Energy
Office of Environmental Restoration and Waste Management
under budget and reporting code KP0101000

OAK RIDGE NATIONAL LABORATORY
Oak Ridge, Tennessee 37831-6285
managed by
LOCKHEED MARTIN ENERGY RESEARCH CORP.
for the
U.S. DEPARTMENT OF ENERGY
under contract DE-AC05-96OR22464

Author Affiliations

This work was originally published as a thesis in partial fulfillment of requirements for a master's degree in nuclear engineering at The University of Tennessee. C. M. Johnson is currently employed by the National Institute of Standards and Technology, Gaithersburg, Maryland.

DISCLAIMER

Portions of this document may be illegible in electronic image products. Images are produced from the best available original document.

CONTENTS

FIGURES

TABLES

ACKNOWLEDGMENTS

I would like to thank my major research advisor, W. H. Casson, for his advisement, encouragement, patience, and, most of all, his friendship. I would like to thank L. F. Miller, my major academic advisor, for his guidance in the pursuit of my degree and for always having such a positive attitude. I thank Bill Robbins, the facility electronic and computer technician, so very much for all of his assistance and his friendship. I thank the Health Sciences Research Division of Oak Ridge National Laboratory, Steve Sims, and Jim Bogard, for providing financial support for my work. Much thanks is bestowed upon Tom Heaton and Tom Fewell of the Food and Drug Administration and Chris Soares of National Institute of Standards and Technology for all of their guidance. I also wish to acknowledge the DOE Office of Health and Environmental Research, which provided funding for the Radiation Calibration Laboratory where the work was done.

ABSTRACT

The proper characterization of an X-ray unit is necessary for the utilization of the source as a dosimetry calibration standard. Upon calibration, the X-ray unit can be used for X-ray calibrations of survey, diagnostic, and reference-class instruments and for X-ray irradiations of personnel dosimeters. It was the goal of this research to provide the Radiation Calibration Laboratory at Oak Ridge National Laboratory with a characterized research X-ray unit that could be used in reference dosimetry. The energy spectra were characterized by performing half value layer measurements and by performing a spectral analysis. Two spectral reconstruction techniques were investigated and compared. One involved using a previously determined detector response matrix and a backstripping technique. The other reconstruction technique was developed for this research using neural computing. A neural network was designed and trained to reconstruct measured X-ray spectra from data collected with a high-purity germanium spectroscopy system. Five X-ray beams were successfully characterized and found to replicate the ANSI N13.11 and the National Institute of Standards Technology X-ray beam codes. As a result, these prepared X-ray beams have been used for reference dosimetry. It has been shown that a neural network can be used as a spectral reconstruction technique, which contributes less error to the lower energy portion of the spectrum than other techniques.

1. INTRODUCTION

1.1 INTENT

Accurate radiation measurements are crucial to the nuclear industry, and they are required by regulatory agencies. The development of a calibration laboratory that is accredited by the National Institute of Standards and Technology (NIST) or is approved by the National Voluntary Laboratory Accreditation Program (NVLAP) is one step of ensuring accurate radiation measurements. According to the draft American National Standard for Dosimetry—Personnel Dosimetry Performance—Criteria for Testing (ANSI N13.11-1993), a dosimeter testing laboratory must be equipped with an X-ray machine in addition to five other calibrated sources.[1]

If properly calibrated, an X-ray unit can provided a calibration laboratory with a wide range of monoenergetic sources. Upon calibration, the X-ray unit can be used for X-ray calibrations of survey, diagnostic, and reference-class instruments and for X-ray irradiations of personnel dosimeters. The goal for this thesis research was to prepare the X-ray facility in the Radiation Calibration Laboratory (RADCAL) at Oak Ridge National Laboratory (ORNL) for NIST accreditation and to developed a new spectral analysis technique.

Although the traditional measures of beam quality, kilovoltage, and half value layer (HVL) have become traditional measures for specifying X-ray beams, these parameters do not provide a complete description of the X-ray spectrum. However, it is doubtful that these measurements will ever be replaced by a complete detailed spectrum. The spectral analysis process is complex, and, in most situations such as in a clinical setting, the amount of information provided by the X-ray spectrum is more than is needed.[2] The additional information obtained through a spectral analysis of the RADCAL X-ray beams was desired to more precisely match the NIST beam codes.

1.2 BASIC X-RAY PHYSICS

Many of the basic properties of X-rays have been known since 1895 when Roentgen first announced the existence of this useful type of penetrating radiation. The modern X-ray tube is based on the Coolidge tube, designed in 1913 by W.D. Coolidge.[3] The X-ray tube components are encased in an evacuated heat-resistant Pyrex glass envelope. The tube is placed in a lead-lined housing, which provides protection against excessive leakage radiation.

The cathode, the electrically negative side of the tube, has two main parts: a filament and a focusing cup. The thoriated tungsten filament, through thermionic emissions, supplies the electrons that are accelerated to a target. Tungsten is generally chosen as the filament material due to its high melting point of 3410°C and tendency against vaporization. One to two percent thorium is added to the tungsten to increase the efficiency of thermionic emission and the life of the tube. The filament is fixed to the metal focusing cap. The purpose of the focusing cup is to condense the electron beam to a small area of the anode.[4]

The anode, the electrically positive side of the tube, has three primary functions. The anode receives electrons emitted by the cathode and conducts them back to the high voltage section of the X-ray machine.[4] The anode, usually fabricated from copper, also serves as a thermal conductor. The portion of the anode struck by electrons, is known as the target. The optimal material of the target is tungsten (or a tungsten-alloy metal) due to its thermal conductivity and high melting point. Additionally, the high atomic number of 79 promotes efficient X-ray production.[4]

When the electrons emitted from the cathode strike the target, more than 99% of the kinetic energy is converted to heat and the remaining energy is involved in the production of X-rays. The constant excitation and relaxation of the outer-shell electrons of the tungsten target result in the emission of infrared radiation.[4] The production of heat increases directly with increasing tube current and almost directly with kilovoltage. The efficiency of X-ray production is independent of current but increases with increasing electron energy provided by the electrical potential between the anode and cathode. Two types of radiation result from this X-ray production: characteristic and bremsstrahlung radiation.

When the electron interacts with an inner-shell electron of the target atom, characteristic radiation results. When a K-shell electron is removed by ionization, the target atom is left in a highly unstable state. When one of the orbital electrons in shell L through P falls into the vacant K shell, an emission of radiation occurs. The X-ray has the energy equal to the difference of the binding energies of the orbital electrons involved. Characteristic X-rays are produced when electrons are ejected from orbits other than the K-shell; however, the energy is insignificant compared to the characteristic X-rays from the K-shell electrons. All of the possible X-rays that are characteristic of the target material form what is known as the discrete spectrum. One's awareness of characteristic X-rays is crucial for spectral analyses and for diagnostic radiographs to which K-shell X-rays contribute significantly.[4]

Bremsstrahlung radiation is produced by the interaction of an electron with the electric field from the nucleus of the target atom. As a result of the influence of the electrical field the electron changes its course and loses some of its kinetic energy. The loss in kinetic energy is accompanied by X-ray emission. Unlike the discrete energies of characteristic radiation, bremsstrahlung radiation is highly nonhomogeneous and can be any energy up to the maximum energy of the interacting electron. The emission spectrum for the bremsstrahlung radiation is known as the continuous X-ray spectrum. The general shape of a continuous spectrum is constant, but the relative position on the energy axis changes. The factors that control the relative position and amplitude are the current and electrical potential of the tube and the amount of added filtration. The greatest number of X-ray photons is emitted with energy approximately one third of the maximum photon energy. The number of photons emitted decreases rapidly at very low photon energies. The effect that each of these factors has on the emission spectrum is described in the following paragraph.

A change in the tube current results in a proportionate change in the amplitude of the spectrum at each energy interval (Fig. 1.1) (ref. 4). A change in the electrical potential of the X-ray tube affects both the amplitude and the position of the spectrum. When the electrical potential is increased, the relative distribution of the emitted photons shifts toward higher energies, as shown in Fig. 1.2 (ref. 4). Adding filtration results in an increase in the effective

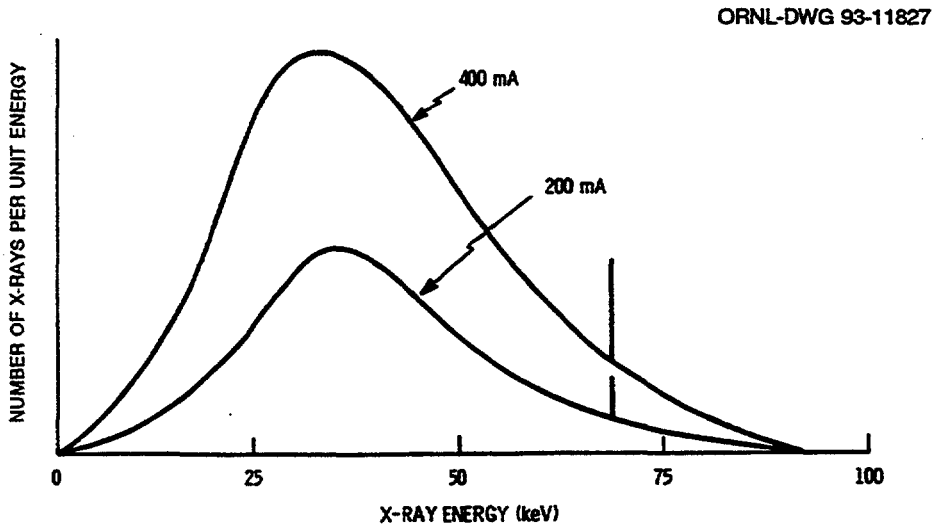

Fig. 1.1. Effect of a change in current on an X-ray spectrum.

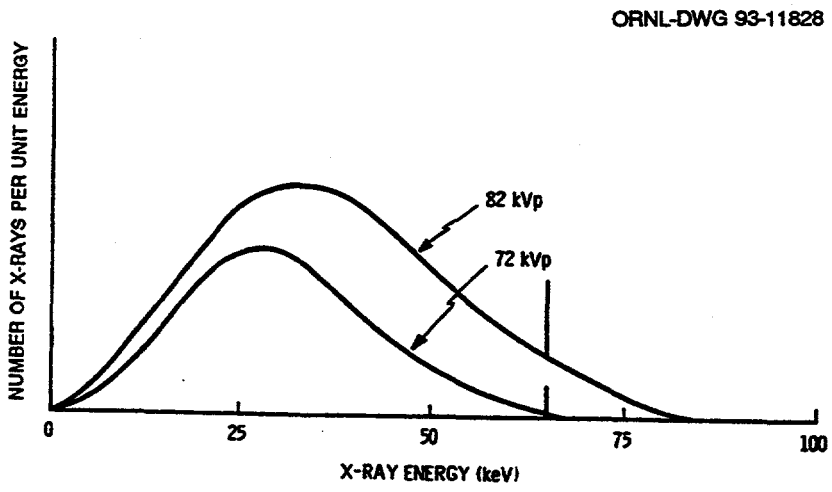

Fig. 1.2. Effect of a change in kilovoltage on an X-ray spectrum.

energy of the X-ray beam and a decrease in the intensity since the filtration more effectively absorbs the lower energy X-rays.[4] The end effect of adding more filtration is a more penetrating beam (Fig. 1.3).

The ideal X-ray spectrum is one of high quality, that is, highly penetrating X-rays. To generate the ideal spectrum, filtration is added to remove the low-energy X-rays. Figure 1.4 shows an unfiltered, normally filtered, and ideally filtered X-ray beam.[4] In an attempt to generate a desirable spectrum, two types of filtration are used: inherent and added filtration. Filtration by the beryllium window and components of the X-ray tube is considered to be inherent filtration. The inherent filtration often increases with age due to the vaporization and deposition of the tungsten target and filament on the tube window.[4] Added filtration is provided by placing additional material in the beam with dimensions that provide a desired degree of attenuation. Aluminum is generally chosen because it is efficient in removing low-energy X-rays through the photoelectric effect. Aluminum is readily available, fairly inexpensive, and can be easily machined or shaped into filters.[4] Copper is another material widely used for added filtration. Tin and lead are also used as filters for the higher energy beams.

In the characterization of X-ray beams the terms X-ray quantity and X-ray quality are encountered. The X-ray quantity is simply another term for the X-ray intensity or radiation exposure measured in roentgens. This is really just a measure of the number of X-rays in the useful X-ray beam. Since the intensity of the radiation changes with distance from the source, measurements are usually given for a certain distance from the anode of the X-ray machine. The X-ray quality refers to the penetrability or the effective energy of the beam. Beams with a high penetrability are termed high-quality or hard and those with a low penetrability are referred to as low-quality or soft beams.[4] In naming the beam codes, NIST has assigned letters that indicate light (L), moderate (M), and heavy filtration (H) and numbers which are equivalent to the constant potential in kilovolts. The X-ray quality is expressed numerically by the HVL, which is the thickness of added filtration required to reduce the X-ray intensity to half its original value. Another term used in expressing the beam quality is the homogeneity coefficient (HC). The HC is the ratio of the first HVL to the second HVL multiplied by 100 (ref. 5). A value for the HC near 100 indicates that the filtration produces an approximately homogeneous beam that is approximately monoenergetic. The simplicity of measuring the HVL makes it the method of choice for expressing beam quality. Measurements of radiation quality are expressed as the HVL of the beam with a certain thickness of filtration and energy.

1.3 VARIOUS RECONSTRUCTION TECHNIQUES

Numerous techniques have been developed to reconstruct spectra from attenuation data. Due to the unavailability of a spectroscopy system in many clinical settings, spectral reconstruction techniques have been developed to use data that would have been previously obtained through parametric description of the beam quality. The Laplace reconstruction approach fits an attenuation curve to an analytical function containing several parameters.[6] If the model is correctly chosen, its inverse Laplace transform is a unique data set that approximates the original spectrum.[6] Another approach is the numerical analysis of the

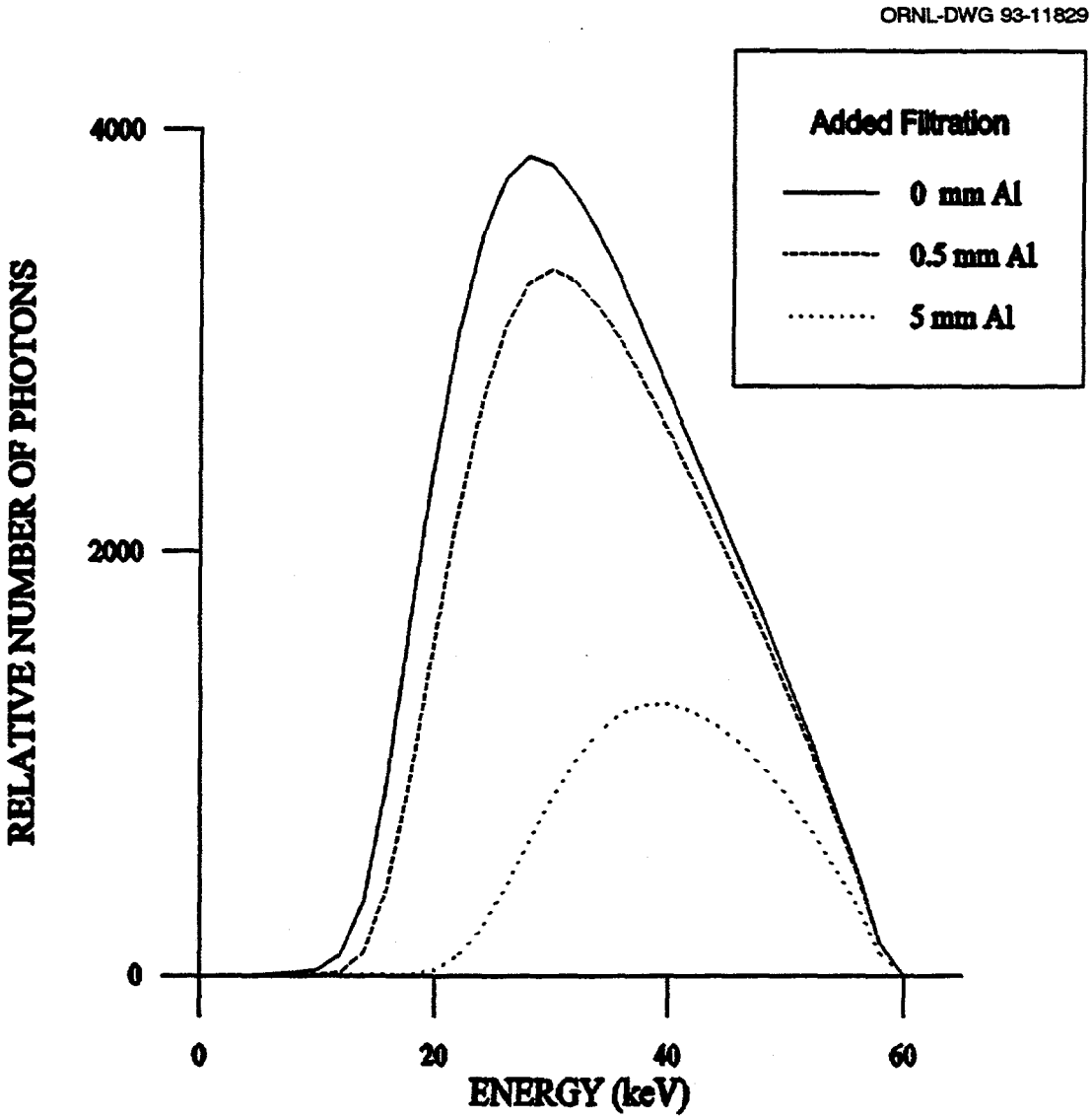

Fig. 1.3. Effect of added filtration on the NIST M60 spectrum.

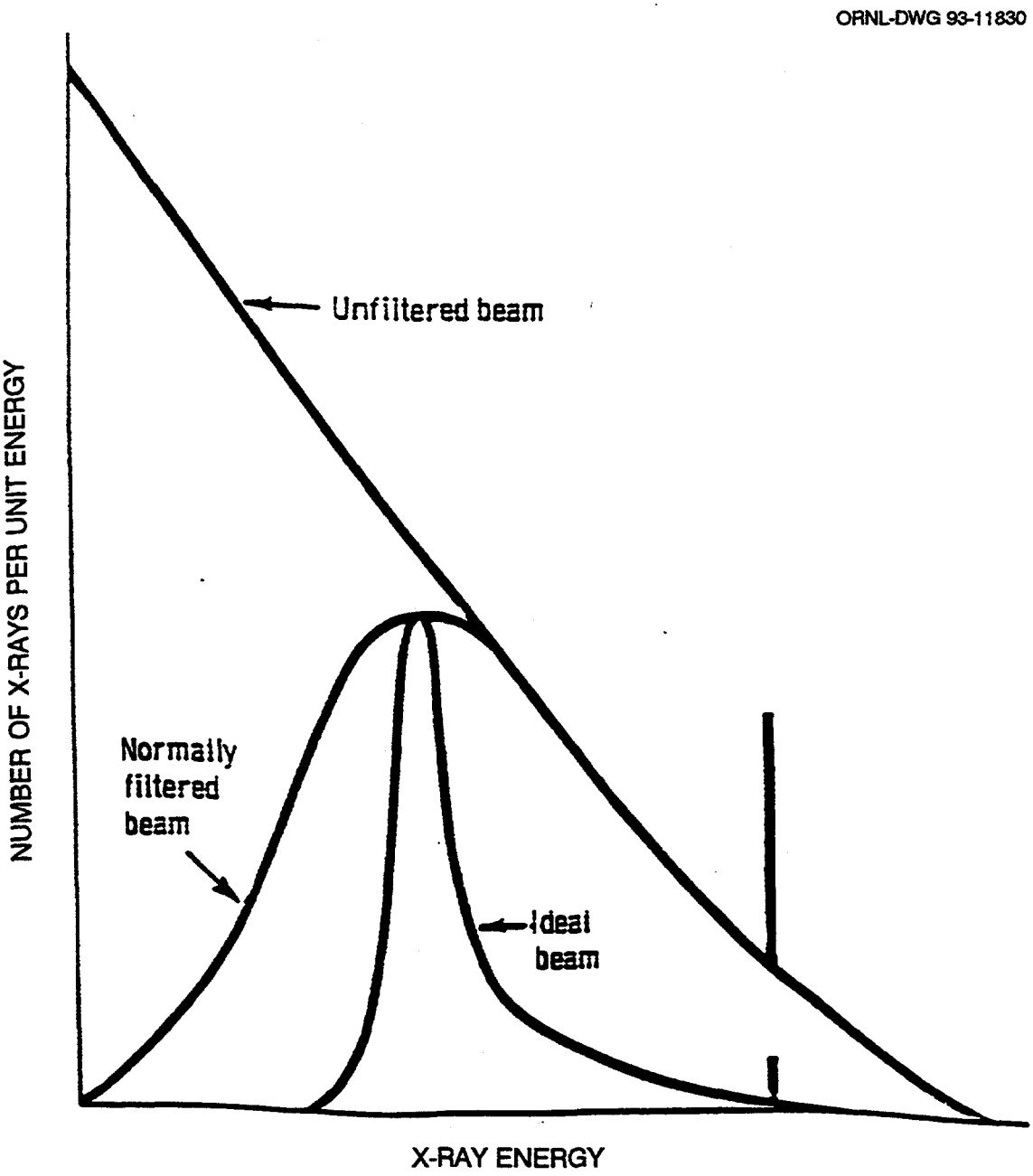

Fig. 1.4. Figure showing the shapes of a typical spectrum with varying amounts of filtration.

transmission data. The principle of this method is to iteratively calculate the spectrum with some sensible physical constraints until the calculated transmission data agree with the measured ones.[7] The response matrix correction technique for this research utilizes a Monte Carlo generated response matrix and backstripping to correct the spectrum for the detector response. This technique is described in detail in Sect. 5.

A spectral reconstruction process using an artificial neural network has been developed as an alternative to other spectral reconstruction techniques. A neural network receives input, processes that input in a highly connected architecture of nonlinear processing nodes, and produces an output.[8] This spectral reconstruction technique is a noniterative approach, in contrast to the numerical analysis and iterative approaches mentioned previously. Additionally this technique does not use attenuation measurements to reconstruct the spectrum. A neural network developed by J. M. Boone produces an energy spectrum from input attenuation data.[2] The neural network developed for the RADCAL work also results in an approximation of an energy spectrum, but it accepts as input data attenuated and unattenuated measured spectra obtained from measurements with a spectrometry system.

2. EQUIPMENT AND MATERIALS

2.1 RADCAL

The Radiation Calibration Laboratory (RADCAL) is operated by the Dosimetry Applications Research (DOSAR) group of the Health Sciences Research Division at Oak Ridge National Laboratory. The calibration laboratory performs work for research groups at ORNL and for private industry. The lab is equipped with several calibrated sources and numerous NIST calibrated instruments. All rooms at RADCAL are environmentally controlled or monitored for humidity, temperature, and pressure.

The X-ray facility, an important feature of RADCAL, is a low-scatter lead-lined room with dimensions of 6.1 × 7.0 × 4.3 m. The room is equipped with an adjustable rail system that extends to 3 m and is used to position and hold the lead collimators, the lead shielding, and the phantom stand. The X-ray source is a 320 kV Pantex X-ray unit with a tungsten target and a 3-mm beryllium window encased in lead housing. The range of electron accelerating potential available with the X-ray unit is ideal for preparing all of the X-ray beams suggested by draft ANSI N13.11–1993, as well as many of the NIST beams. A beryllium window with a thickness of 3 mm was chosen for this work, in order to duplicate one of the X-ray units used at NIST for calibration purposes.

2.2 COLLIMATION

The X-ray beam is collimated with a series of half-inch thick, 20- by 20-cm lead sheets. For the HVL measurements, the first collimator, with an opening of 9 by 9 cm^2, is placed 0.45 m from the anode. The second collimator, with an opening of 20 by 20 cm^2, is placed 1.5 m from the anode. A diagram of the collimation is found in Fig. 2.1. The placement of these collimators with the apertures as described results in a fully exposed 15-cm thick, 30- by 30-cm polymethylmethacrylate phantom whose front face is located at a distance of 3.17 m and centered on the X-ray beam. The collimation was altered for the spectral analysis, as discussed in a later section of this work.

2.3 IONIZATION CHAMBER

All of the X-ray beam calibration measurements were made with an Exradin A-2/A-3 ionization chamber and with a NIST-comparable Keithly 617 electrometer. The following description was found in brochures from Exradin. The A-3 chamber is a spherical air-equivalent chamber based on the Shonka-Wyckoff design. The chamber is mounted to a low-noise triaxial cable. The chamber is constructed entirely of air equivalent conducting plastic, with a collecting volume of 3.6 cc and a wall thickness of 0.25 mm and an optional 2.0 mm equilibrium cap. This chamber was originally conceived to serve as a secondary standard instrument. The A-3 chambers are widely used in diagnostic radiology, radiation protection, and research and are well suited for beam calibrations, quality assurance, and dose assessment.

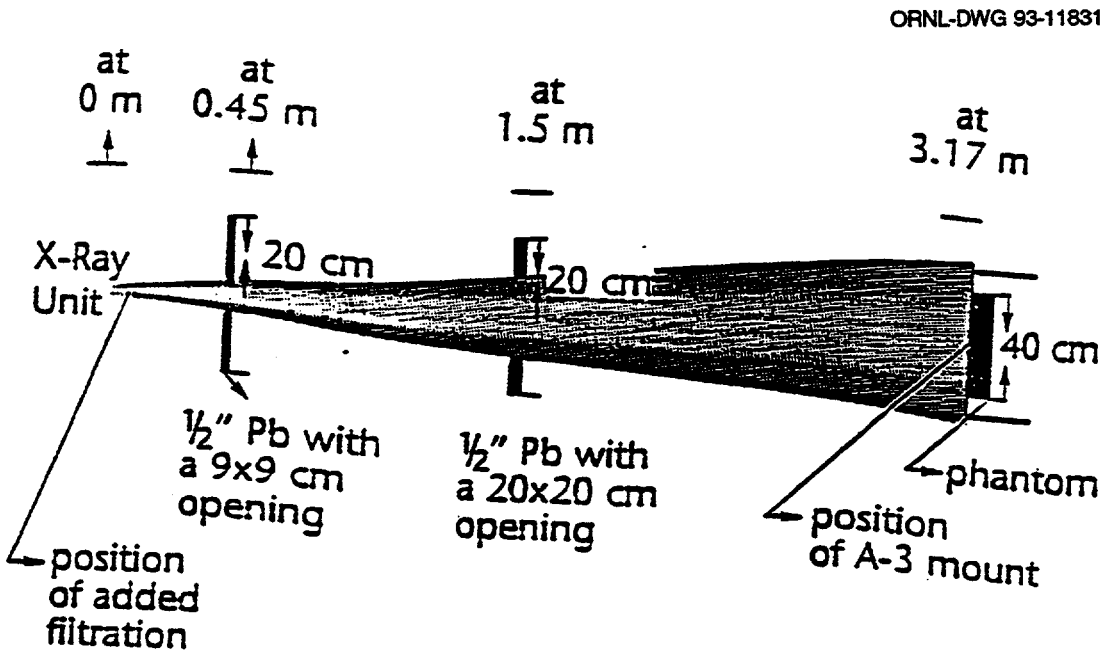

Fig. 2.1. Diagram of collimator set-up in X-ray facility.

The RADCAL facility has three A-3 chambers, two of which are NIST-calibrated for several X-ray beams. In order to directly obtain a calibration factor for each of the X-ray beams of interest, the reference A-3 ion chamber would need to be calibrated to more NIST X-ray beams. Additionally, the calibration factor is a function of the HVL of the X-ray beam. Since the HVL changes with every addition of filtration, a method for calculating the calibration factor was necessary to this work. The mathematical relationship used for determining the calibration factor was made available by T. Heaton, presently of the Food and Drug Administration (FDA). In his previous position at NIST, he compiled all the calibration factors for all of the A-2 chambers calibrated at NIST. A description of his work is found in an unpublished manual titled *Secondary-Level Laboratories: Methodology for a Calibration Program*, from which the following information was obtained.[9] Since the majority of these chambers were calibrated to the M100 beam, the calibration factors for all of the other beams were normalized to the value for the M100 beam. The resulting calibration factor is referred to as the relative calibration factor and is found graphically in Fig. 2.2 (note the mathematical relationship also found on the graph).

2.4 HIGH PURITY GERMANIUM DETECTOR

Spectrometry was performed with a high purity germanium (HPGe) planar detector and a multichannel analyzer (MCA) system. An EG&G ORTEC Model GLP-11190-S LEPS series HPGe planar low energy photon detector was purchased for use in this work, upon the recommendation of C. Soares of NIST and T. Fewell of FDA. The planar detector has an ultra-thin ion implanted boron front contact and a 0.0254 mm beryllium window. The active area is 100 mm^2 with a sensitive depth of 10 mm and a diameter of 11.3 mm. The detector-to-entrance window distance is 7 mm. The guaranteed resolution is 190 eV full width at half maximum (FWHM) at 5.9 keV for ^{55}Fe and 550 eV FWHM at 122 keV for ^{57}Co. These two isotopes were used to establish known peaks for the calibration of the MCA. A linear relationship was assumed between the energies of the ^{55}Fe and ^{57}Co peaks and the channel numbers of the peaks. Through changes in amplification the MCA was calibrated to 0.1 kev per channel.

2.5 FILTERS

The majority of the copper (Cu) and aluminum (Al) filters used to make the attenuation measurements and the attenuators used in the spectral analysis have a purity of 99.99%. The exception are the Al filters, which measure less than 0.05 mm. These have a purity of 99.5%. Tin and lead filters were used for several of the higher energy beams. No significant errors are expected due to the use of the slightly lower purity material. However, when taking HVL calibration measurements, the purity of the Al and Cu must be taken into account. Small amounts of impurities have been shown to degrade the accuracy of the reconstructed spectrum.[10] For example, Al 1100, which is an alloy required to contain 99% Al, has been found to interfere with an accurate spectral analysis.[10] The possible contaminants of the aluminum 1100 are iron, silicon, copper, manganese, and zinc. The reason a low percent impurity, such as 1%, can cause such inaccuracies is because the atomic numbers of these impurities are quite different from that of Al, resulting in different attenuation qualities. Of

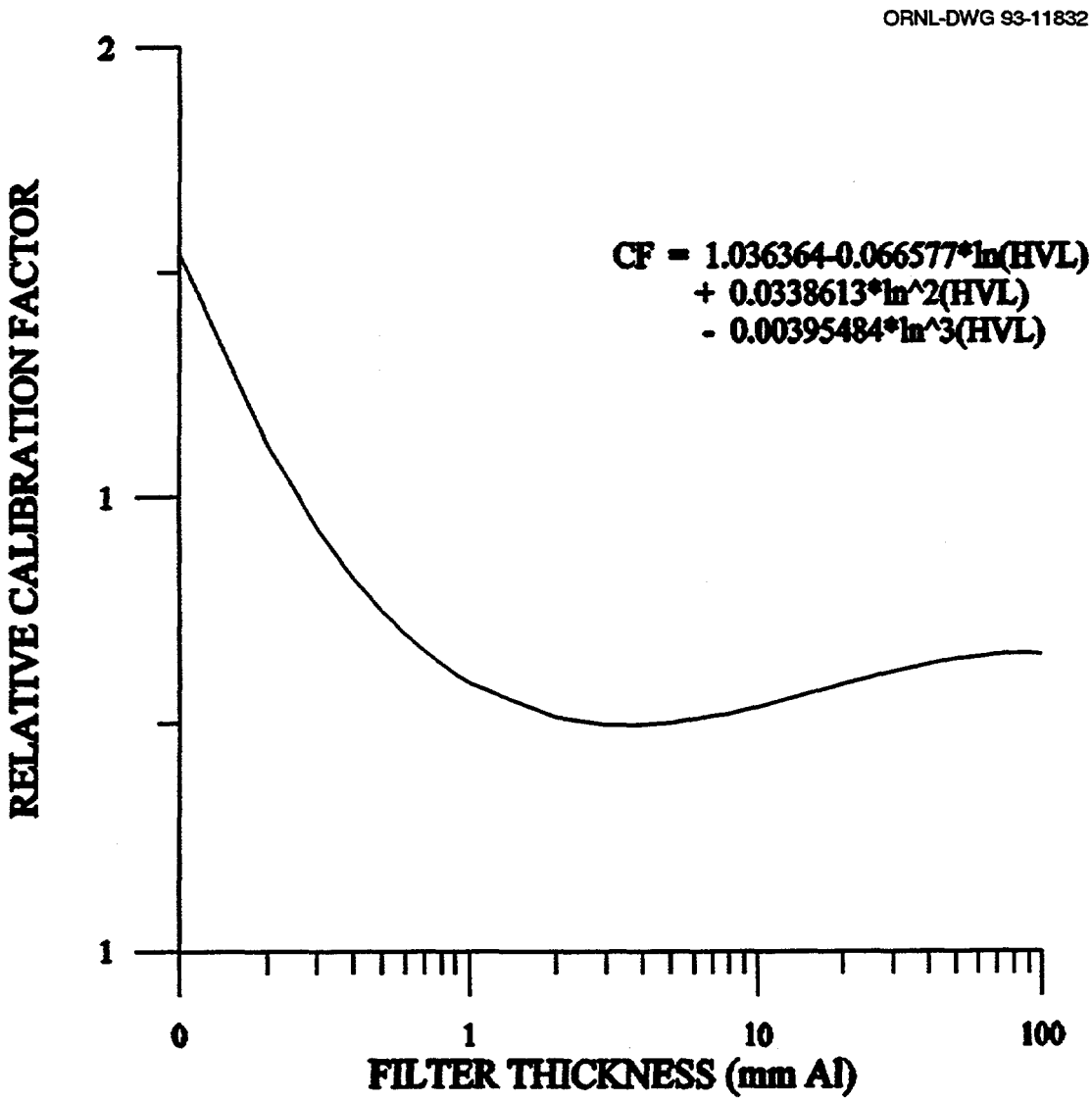

Fig. 2.2. Relative calibration factors for the Exradin ion chamber.

all these impurities only silicon is close in atomic number to Al. If the exact impurities are known, a correction can be made by taking into account the mass attenuation coefficient of the impurity. A correction for the effects of the impurities is found in Appendix A of Archer and Wagner (ref. 10).

In addition to the purity of the material, the thickness must be accurately measured. Although the thickness of each filter was quoted by the manufacturer, all of the filters were remeasured with a precise micrometer and found to differ significantly in thickness from the stated measurements. A Mitutoyo digital micrometer, with a resolution of 0.001 mm was used to obtain an averaged value from a series of measurements for each of the 2- by 2-in. filters. The uncertainty associated with these precisely measured filters is considered to be negligible.

2.6 XCOM

XCOM is a computer program and database prepared by M. J. Berger and J. H. Hubbell of NIST. The XCOM program will calculate photon cross sections for scattering, photoelectric absorption, and pair production and will determine mass attenuation coefficients for any element, compound, or mixture at any energy in the range of 1 keV to 100 GeV. The main program consists of various FORTRAN subroutines that, upon requesting the user to specify the chemical symbols for the composition of the material and the desired energy grid, generate coefficients for cubic-spline fits. All coefficients used in this research were obtained by using XCOM. A graph of the Al attenuation coefficients is found in Fig. 2.3. The program is extremely user friendly, prompting the user for simple requests and preparing a straightforward output.

2.7 HVL CODE

The HVLs for the X-ray beams were calculated by using a computer code written by H. T. Heaton of FDA. The code was designed to be used by secondary-level ionizing radiation calibration laboratories. Through the use of this computer code the laboratories gather data in a prescribed manner. The computer code includes programs for calibration procedures for several classes of instruments using equipment common to state sector laboratories and for quality control of the calibration equipment. There are also programs for making measurements necessary to determine the various uncertainty components of the calibration. The majority of the code was not relevant to the X-ray beam calibration at RADCAL. The appropriate thickness of additional filtration and the accompanying HVL can be determined by the portion of this code which calculates a calibration factor for an A-3 chamber as a function of the HVL of the X-ray beam. The database used in determining these calibration factors was obtained from all A-3 chambers calibrated at NIST, as described previously in this work. Appendix C contains a description of the HVL code as found in the manual contributed by T. Heaton, *Secondary-Level Laboratories: Methodology for a Calibration Program.*[9]

The code can be used to start the calculations with no added Al filtration or the user can select a different starting point on the transmission curve, subtracting the amount of Al at

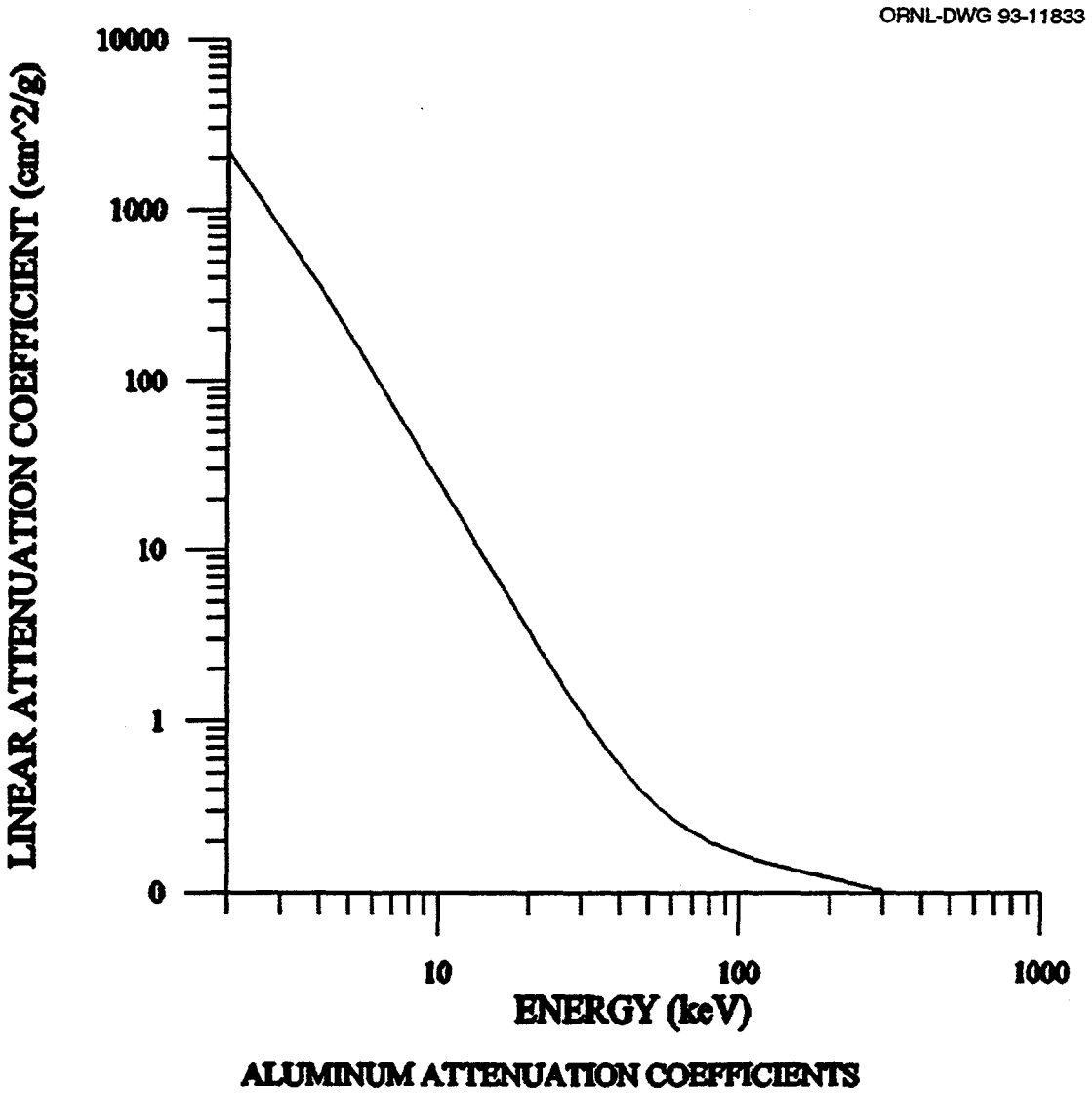

Fig. 2.3. Aluminum attenuation coefficients.

that point from the rest of the values of added Al. For each of the starting points a "new" base filter pack is effectively created and the code calculates the HVL and HC for that beam. Therefore, the HVL can be calculated for several base filters from only one measurement.

3. CALIBRATION OF X-RAYS BEAMS

3.1 NIST CRITERIA

The goal of the calibration and characterization of various X-ray beams produced by the RADCAL X-ray unit was to meet requirements for a Secondary Calibration Laboratory Accreditation by NIST. Throughout the preparation process all of the NIST criteria for accreditation were implemented whenever possible. The NIST criteria are provided in full detail in NIST publication 812 in parts A and C-2 (ref. 11). The criteria included in this work summarize the criteria that are relevant to the development of the procedures for the calibration of X-ray beams for the irradiation of personnel dosimeters.

The criteria require there be at least one constant-potential X-ray generator available to cover a range of exposures for protection-level irradiations, with a minimal range of 30 mR to 500 R (0.3 mGy to 4 Gy). Three or more of the NIST beams codes described in ANSI N13.11 and DOE/EH-0027 must be available for irradiations. The leakage through a closed shutter shall be less than 0.1% of the open-shutter rates at the position of the dosimeters, and the shutter transit time must be known.

The X-ray beams must be collimated, and their size limited to an area as specified by the irradiation requirements. All dosimeters should be uniformly irradiated with phantom backing, using a beam size sufficient to fully irradiate the phantom face. A polymethylmethacrylate phantom with a minimum surface size of 30 by 30 cm and a thickness of 15 cm should be supported on a sturdy minimum-scatter support system. The dosimeters should be placed at least 5 cm from the edge of the phantom, at a distance of at least 1 m from the anode of the X-ray tube.

The radiation field should be characterized in terms of exposure rate in the absence of the phantom at the location where the center of the front surface of the phantom is placed for irradiation, and the contribution from room scatter radiation should be measured with the phantom removed. The scatter should not exceed 5% of the exposure rate at any location where a dosimeter would be placed. The X-ray beam emitted from the tube housing should be filtered to achieve an appropriate radiation quality for calibration purposes.

The beam quality should be expressed in terms of the HVL and HC. The first HVL and the HC for a given beam should be within 5 and 7%, respectively, of the values found in Table 1, Characteristics of X-ray Beams, in Sect. B.2.6 of NIST Publication 812. Five of the NIST beam codes have been chosen as test spectra by the ANSI for dosimeter testing. The graphical representations of these five spectra, as found in the ANSI N13.11-1993, were reproduced and are found in Fig. 3.1. The characteristics of the beam codes duplicated for this work are presented in Table 3.1. The electron accelerating potential and the additional filtration can be adjusted in order to approach the target HVL and HC, as long as the X-ray intensity does not vary more than 5% across the useful area of the beam.

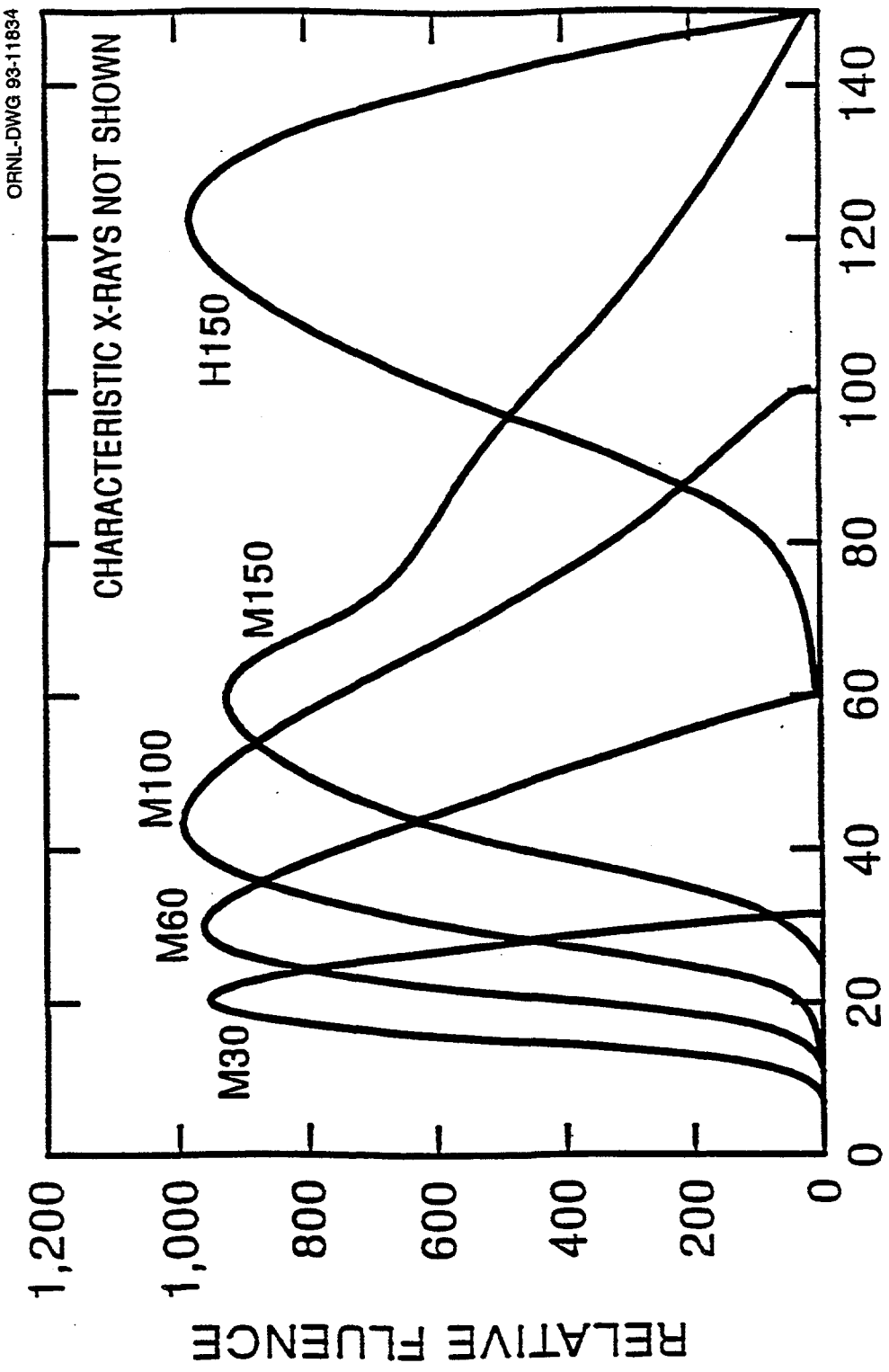

Fig. 3.1. The five NIST spectra chosen to be test spectra for dosimeter testing.

Table 3.1 Characteristics of X-ray beams investigated

Radiation source							Conversion factors[a]			
NIST[b] beam code	Added filter (mm)			HVL[c]	HC[d]	Average energy	Deep	Shallow	Deep	Shallow
new	Al	Cu	Sn	(mm Al)		(keV)	old[e]	old[e]	new[f]	new[f]
M30[g]	0.5			0.36	0.64	20	0.40	0.92	0.47	1.04
M60[g,h]	1.51			1.68	0.68	34			1.07	1.30
S60	2.50			2.79	0.79	36	0.98	1.14		
S75	1.5			1.86	0.63	39	0.95	1.14		
M100[g]	5.0			5.03	0.73	51	1.20	1.30	1.65	1.62
M150[g]	5.0	0.25		10.25	0.89	70	1.38	1.43	1.92	1.78
H150[g,h]	4.0	4.0	1.51	17.0	1.00	117			1.80	1.73

[a]For complete definition of conversion factors see ANSI N13.11–1993.
[b]National Institute of Standards and Technology.
[c]Half value layer.
[d]Homogeneity coefficient.
[e]"Old" refers to ANSI N13.11–1983.
[f]"New" refers to ANSI N13.11–1993.
[g]Beam codes chosen for the revised ANSI N13.11-1993.
[h]Beam codes not listed in ANSI N13.11-1983.

3.2 PROCEDURE FOR MEASURING BEAM QUALITY

After collimating the X-ray beam as described in Sect. 3, the first parametric measurement made was to test for beam uniformity. It was not necessary to measure the room scatter or the leakage through the closed shutter. These measurements had been made previously and were found to meet the NIST criteria. An investigation of beam uniformity was performed by taking measurements of the M150 beam with an A-3 ion chamber. The chamber was placed in positions that varied vertically and horizontally across the phantom stand. The results of these measurements are found in Fig. 3.2. The NIST criteria were met for this measurement since the beam intensity did not vary more than 5%.

The next step in calibrating an X-ray beam is to evaluate the HVL of a beam that has been filtered. The beam used as the example beam for this discussion is the S75 beam. This is one of the special beams developed by NIST for DOE facilities to use in dosimetry. Although the NIST criteria allow the voltage to be altered in order to match the beam codes, in this work only the filtration was varied. Throughout the collection of the measurements for the S75 beam, the target potential was 75 keV.

A series of attenuation measurements were made by placing different thicknesses of Al in the X-ray beam. In addition to a measurement with no added Al, ten different combinations of added filtration were used. The filters chosen and the corresponding collected data are shown in Table 3.2. When deciding on which filters to use, the beam under investigation and the strength of the signal is considered. If a significant signal can be measured, measurements should be made through ten HVLs. Measurements should be obtained using several filters with a thickness close to the NIST suggested HVL. At least four different filter measurements should be made above and below the probable HVL. The suggestions on which combinations of filters to use were those of T. Heaton. The measurements made near the HVL, on which small iterations are made, help to provide more data in the region of the HVL and better evaluate the true HVL.

Generally, 10 to 20 1-min data points were obtained for each filter thickness, except for the thicker filters where often 30 or more 1-min data points were obtained. The A-3 response was measured by an electrometer and recorded through a computer interface. A computer program, which corrected the measurements for temperature and pressure, was used. In addition to the environmental corrections made to the collected charge, the data were averaged and the coefficient of variation calculated to serve as a check for counting statistics. Generally, the percent standard deviation for the charge collected was kept below 1%. After obtaining an averaged corrected measurement of the charge collected per minute in units of coulomb per minute (C/min) for each filter, the data were combined in an ASCII file in the appropriate format to be used as input for the HVL code.

Heaton's HVL code was used to evaluate a HVL and HC for each different base filtration listed in Table 3.3. The percent differences from the NIST HVL and HC for each of the base filter combinations were evaluated and then plotted in an attempt to find the optimal filter thickness. These results are found on Fig. 3.3. In choosing the optimal filter thickness an attempt is made to keep the percent difference from the NIST value for both the HVL and HC to a minimum. From Fig. 3.3 it was determined that a base filter of

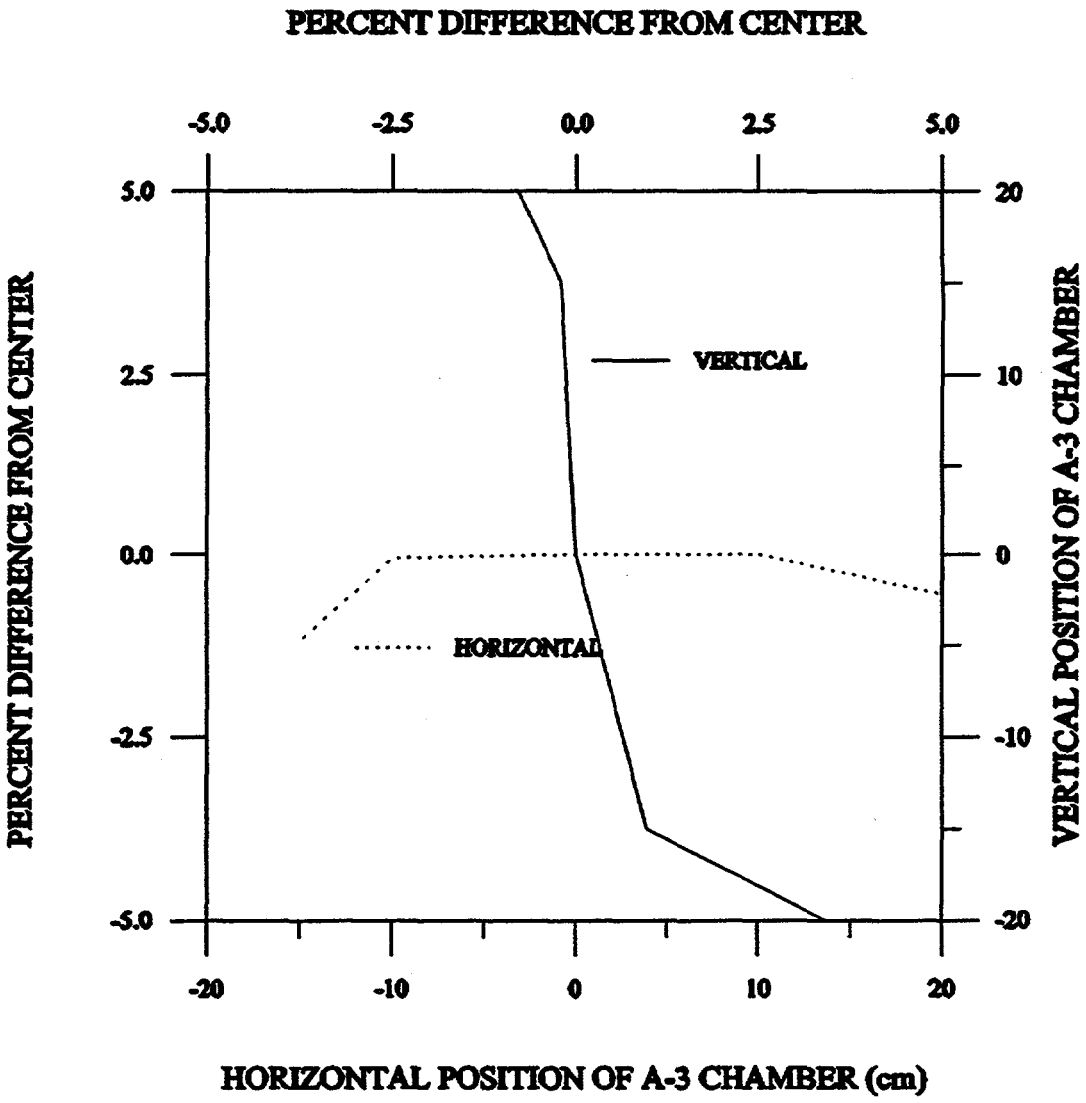

Fig. 3.2. Horizontal and vertical beam profile. (The horizontal positioning corresponds to the bottom and the left axes and the vertical positioning corresponds to the top and the right axes.)

Table 3.2. Data for determining HVL[a] for the S75 beam

Added aluminum filtration (mm)	Uncorrected charge rate (C/min)[b]	Corrected charge rate (C/min)[b]	Percent standard deviation
0.000	6.626×10^{-9}	6.811×10^{-9}	0.008
0.186	4.235×10^{-9}	4.345×10^{-9}	0.363
1.038	1.947×10^{-9}	2.002×10^{-9}	0.199
1.503	1.546×10^{-9}	1.588×10^{-9}	0.351
1.740	1.390×10^{-9}	1.427×10^{-9}	0.167
2.018	1.217×10^{-9}	1.253×10^{-9}	0.240
3.056	8.688×10^{-10}	8.944×10^{-10}	0.435
3.426	7.794×10^{-10}	8.023×10^{-10}	0.361
5.117	5.282×10^{-10}	5.437×10^{-10}	0.388
9.950	2.310×10^{-10}	2.381×10^{-10}	0.526
20.141	7.332×10^{-11}	7.558×11^{-11}	0.266

[a]Half value layer.
[b]Coulomb per minute.

Table 3.3. Initial results of the HVL code for the S75 beam

Added aluminum filtration (mm)	Resulting HVL[a] (mm)	HC[b]
0.000	0.75	0.46
0.186	0.70	0.45
1.038	1.61	0.58
1.503	1.99	0.61
1.740	2.19	0.63
2.018	2.44	0.66
3.056	3.06	0.71
3.426	3.18	0.69
5.117	3.92	0.73

[a]Half value layer.
[b]Homogeneity coefficient.

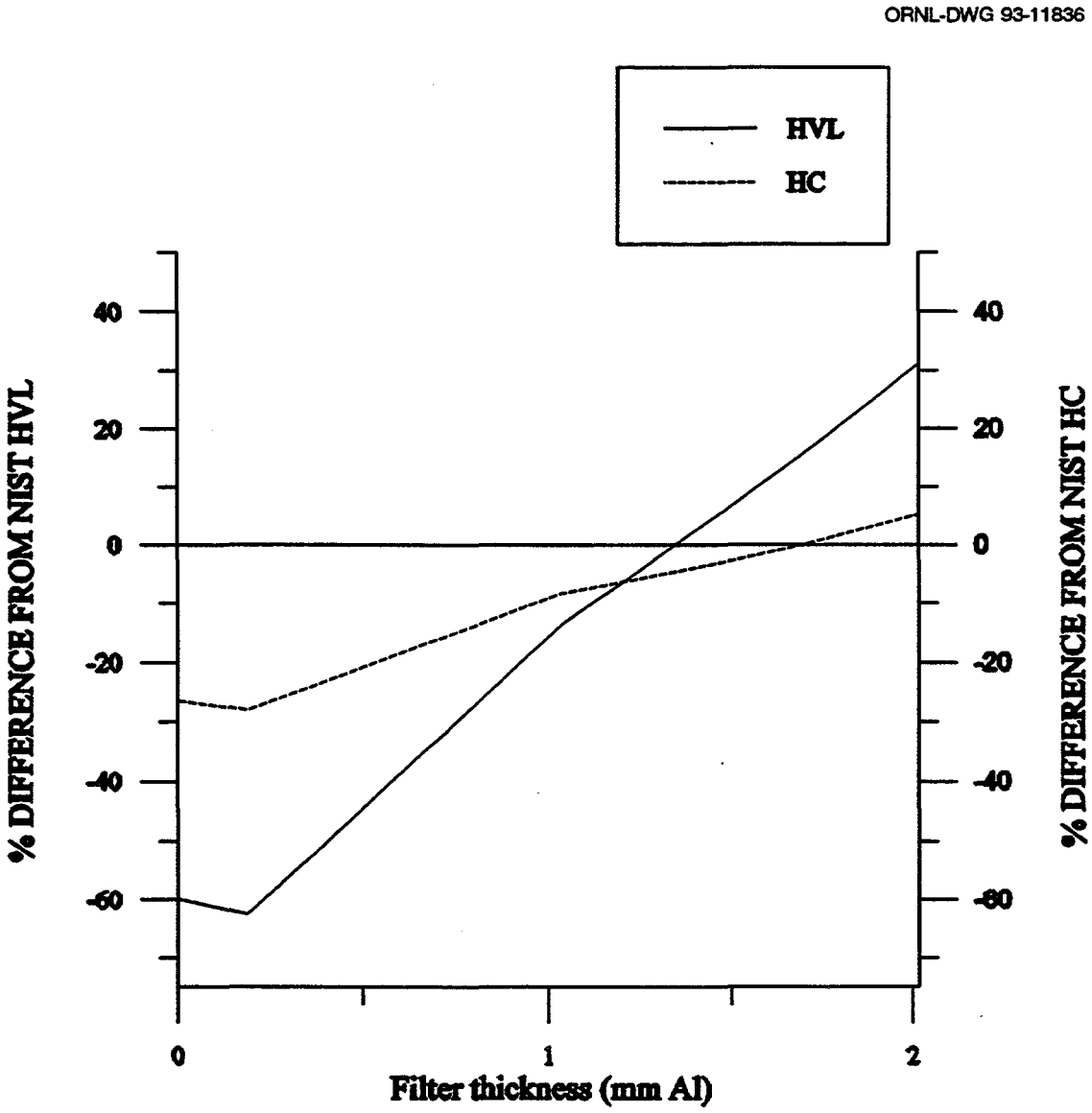

Fig. 3.3. Evaluation of optimal filter thickness for the S75 X-ray beam.

1.34 mm Al would be the most appropriate choice for matching the NIST beam.

A verification procedure was then used to test whether the 1.34 mm Al base filtration did indeed have an HVL and HC of an S75 beam. Using the 1.34 mm Al filter as the base filtration, another series of attenuation measurements was made. These filter thicknesses and the corresponding corrected measurements are found in Table 3.4. Again these data were used as input for the HVL code to evaluate an HVL and HC for a base filtration of 1.34 mm Al. The results for the S75 beam follow in Table 3.5. It is important to understand that the effect of filter thickness on response of the A-3 ion chamber (as described in Fig. 2.2) must be taken into account. When the attenuation data were plotted and the first HVL evaluated from this graph (Fig. 3.4), an HVL of 3.1 mm Al was found for the S75 beam with a base filter of 1.34 mm Al. This is significantly higher than that found when the A-3 response was corrected for the effects of the filter.

The complete procedure, as described above, for determining the beam quality was performed on four other beams. The results follow in Table 3.6.

Table 3.4. Data used for the verification of 1.34 mm Al base filtration

Base filter: 1.34 mm Al + added aluminum filtration (mm)	Uncorrected charge rate (C/min)[a]	Corrected charge rate (C/min)[a]	Coefficient of variation (%)
0.000	1.664×10^{-9}	1.719×10^{-9}	0.378
0.519	1.322×10^{-9}	1.365×10^{-9}	0.266
0.703	1.233×10^{-9}	1.274×10^{-9}	0.207
2.028	8.002×10^{-10}	8.272×10^{-10}	0.589
5.117	4.049×10^{-10}	4.185×10^{-10}	0.354
7.145	2.874×10^{-10}	2.971×10^{-10}	0.271
9.950	1.923×10^{-10}	1.987×10^{-10}	0.152

[a]Coulomb per minute.

Table 3.5. Results from the parametric measurements of the S75 beam

	NIST[a] suggested values	Measured values	Percent difference from NIST
Base aluminum filtration (mm)	1.504	1.34	
HVL[b] (mm)	1.86	1.89	1.61
HC[c]	63	62	-1.58

[a]National Institute of Standards and Technology.
[b]Half value layer.
[c]Homogeneity coefficient.

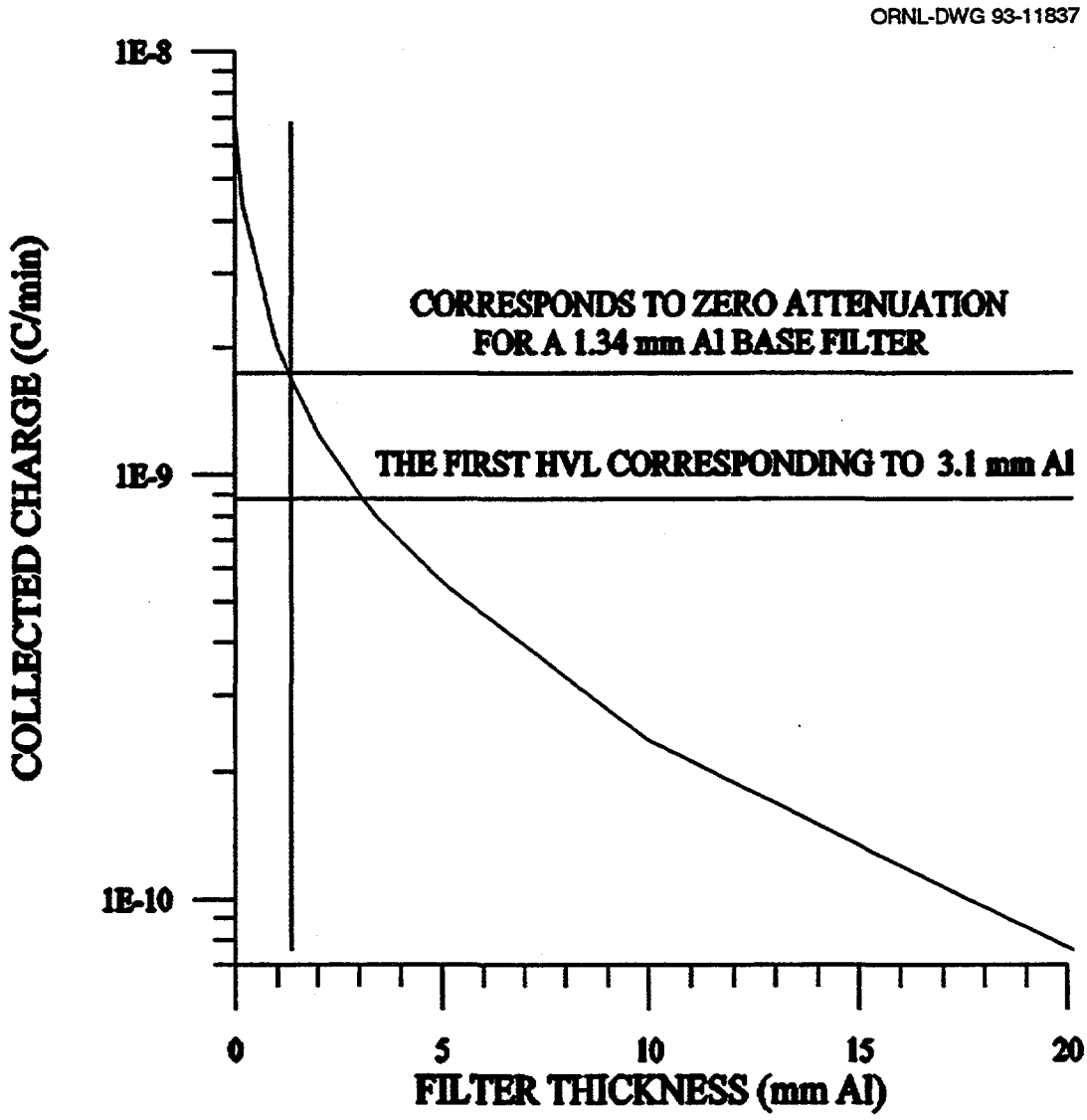

Fig. 3.4. Attenuation curve for the S75 beam.

Table 3.6. Results of parametric measurements

X-ray beam code	Average energy (keV)	NIST[a] values			Measured values for RADCAL[b]			Percent difference from NIST[a]	
		Base aluminum filter (mm)	HVL[c] (mm)	HC[d]	Base aluminum filtration (mm)	HVL[c] (mm)	HC[d]	HVL[c]	HC[d]
M30	20	0.50	0.36	0.64	0.186	0.368	0.634	2.2	−0.94
M60	34	1.51	1.68	0.68	1.557	1.69	0.66	0.59	−2.94
S75	39	1.504	1.86	0.63	1.34	1.89	0.62	1.61	−1.58
M100	51	5.0	5.03	0.73	5.117	5.16	0.72	3.2	−0.64
M150	70	5.0[e]	10.25	0.89	5.084[f]	10.33	0.86	1.27	−1.05

[a]National Institute of Standards and Technology.
[b]Radiation Calibration Laboratory.
[c]Half value layer.
[d]Homogeneity coefficient.
[e]0.25 mm using copper filter.
[f]0.233 mm using copper filter.

4. DETECTOR RESPONSE MATRIX CORRECTION TECHNIQUE

4.1 INTERACTIONS WITH DETECTOR

The difficulty in obtaining spectral measurements arises from the high count rates that are characteristic of these high energy photons. Typically, the lowering of the count rate is achieved through the use of collimators, shielding, and current adjustments. A dead time less than 10% was considered acceptable for these measurements. The lead collimators remained in the same position for the spectral measurements as that used for the HVL measurements (see Sect. 2.2, Fig. 2.1). Two half-inch lead sheet collimators with 4- by 4-in^2 openings were placed adjacent to the previously placed lead sheet collimators. Of course this altered the beam spread on the phantom, but having a fully exposed phantom is not important for the spectral analysis. The HPGe planar detector, wrapped with lead sheets, is placed at a horizontal distance of about 3.7 m from the X-ray focal point. Lead bricks and a lead pinhole collimator were placed around the detector to provide additional shielding. The first seven attenuator measurements, 0 to 0.5 mm Al, were made with a X-ray machine current setting of 0.5 mA. An increase in current was necessary for the thicker attenuator measurements in order to obtain a significant signal. The current was increased to 5 mA for the 5-mm Al measurement and to 20 mA for the 10- and 20-mm Al measurements.

An accurate X-ray spectrum is necessary in order to fully characterize the X-ray beam. Since these spectra were measured experimentally, it was necessary to make appropriate corrections to the pulse height distribution to reconstruct the true incident photon energy spectrum. The majority of the distortions occur because the primary photons are partially absorbed or escape completely before being detected. A paper by Seltzer,[12] which discusses the calculated response of HPGe detectors, and papers by Chan et al.[13] and Chen et al.,[14] which discuss the determination of the response of HPGe from Monte Carlo methods, present excellent overviews of the response of typical germanium detectors used in X-ray spectrometry. The mechanisms that cause the detected energy to be lower than the true incident photon energy are the escape of characteristic X-rays resulting from photoelectric absorption events in the Ge K-shell and the escape of the incident photons scattered to lower energies in Compton collisions.[12] The probabilities for an incident photon to be counted in the different energy channels depend on the incident energy, detector dimensions, and the irradiation geometry. Monte Carlo calculations tabulate the energy response relative to the number of incident photons in the following categories: (1) photopeak efficiency, (2) K_α or K_β escape fraction, (3) Compton fraction, (4) penetration fraction, and (5) elastic escape fraction.[13]

The photopeak efficiency reflects the relative number of photons that deposit all of their energy in the detector. The photopeak efficiency increases with area and thickness of the detector crystal. However, for low-energy photons with short mean free paths the photopeak efficiency is almost independent of the dimensions of the crystal.[13] Increasing the thickness of the crystal, which reduces the penetration, is much more effective than increasing the area for an improvement of the photopeak efficiency.[13]

The K escape fractions result from the photons that deposit all their energy, except for the K_α or K_β X-ray of the germanium. The K escape fraction is approximately 16% at the K edge of germanium, and it decreases to only 1% at 50 keV.[14] K escape is probable only for X-rays produced very near a surface, since in Ge these photons have a mean free path of only 50 μm.[12] These fractions are independent of the detector dimensions and are relatively constant among detectors since the majority of the K escape photons originate from a small volume close to the crystal's surface.[13] The probability of K X-ray production close to a surface is high for low-energy photons, which are photoelectrically absorbed near the entrance face.[12]

The Compton fractions result from the photons that deposit only part of their energy by inelastic scattering and then escape. The Compton fraction decreases with increasing detector area due to the reduction of the photons escaping from the side of the detector.[13] For a given area the detector thickness dependence varies with the incident photon energy. The Compton fraction is essentially constant at low energies while it increases at medium energies due to the reduction in the number of photons scattered in the forward direction. The Compton fraction increases at high energies because the increase in detector thickness reduces the penetration fraction, so the number of photons which contribute to the Compton fraction increases.[13] At energies above 100 keV the Compton fraction is considered to increase with both photon energy and detector thickness.[14]

The penetration fraction is defined as those photons that pass through the detector crystal with no interaction. The elastic escape fraction results from photons that undergo single or multiple coherent scattering events before escaping the detector.[12] These elastic escape photons can be viewed the same as the penetration fraction photons, since neither deposit their energy. The elastic escape contribute only a few percent of the total when the energy of the incident X-ray is less than 150 keV.[13]

4.2 DETECTOR RESPONSE MATRIX

This spectral correction method performs backstripping on the collected MCA data. The response matrix for the planar HPGe was developed through the Monte Carlo calculations performed by Chan et al. (ref. 13). Two thorough descriptions of the response matrix are found in the work by Chan et al. (ref. 13) and in the *Handbook of Computed Tomography X-ray Spectra* by Fewell et al. (ref. 15). Each row of the response matrix is the response of the detector to a monoenergetic photon. The column values in the row gives the probability of detecting the monoenergetic photon in each 2 keV interval up to the maximum energy interval. The diagonal values of the response matrix are the values of the photopeak efficiencies. The sum of the probabilities in each row is the probability that the monoenergetic photon will interact with the detector and be registered as a count.

4.3 BACKSTRIPPING

A summarized description of the backstripping correction procedure follows, with a more detailed description following in Appendix B. The information was obtained in part from the

appendix of Chan et al. (ref. 13). The correction begins at the high-energy end of the spectrum where there are no interactions due to K escape nor Compton contributions from higher energy photons. The counts in this interval can only be due to the photopeak efficiency of the detector. The true number of incident photons at this energy can be determined by dividing the counts in this interval by the photopeak efficiency. This true number of incident photons at a particular energy is multiplied by the K_α and K_β escape fractions, or by the Compton fraction, to determine the magnitude of the K escape peaks and the Compton distribution. The K escape peaks and energy degradation by Compton scattering result from the incomplete absorption of the incident photons at a particular energy. These photons are not registered against their true energies, but contribute instead to the number of events registered at lower energies. The K_α and K_β escape peaks and the Compton continuum are predicted by Monte Carlo analysis and subtracted from the energy region of interest. This correction provides the correct number of counts in the region of interest and provides Compton and K-escape contributions to lower energies. This backstripping is repeated for each lower energy interval.

The computer program contributed by T. Fewell* performs this backstripping procedure. The code was designed to accept data from an MCA calibrated with each channel equalling 0.1 keV and bins the data in 2-keV intervals. In addition to correcting the spectrum through the backstripping procedure, the code normalizes the spectrum for plotting, calculates the HVL from the spectrum, and determines the exposure if desired.

The backstripping procedure results in a corrected spectrum with the following two features. First, in the high energy region the measured pulse height distribution (PHD) is low due to the incomplete absorption of photons by the detector. Second, in the low energy region the measured PHD is high due to the Compton continuum and K escape photon contributions resulting from the higher energy incident X-rays.[13] The results of this correction code can be seen in Fig. 4.1, which shows the effect of backstripping on the RADCAL M30 spectrum.

*T. Fewell, Food and Drug Administration, personal communication to C. M. Johnson, January 1993.

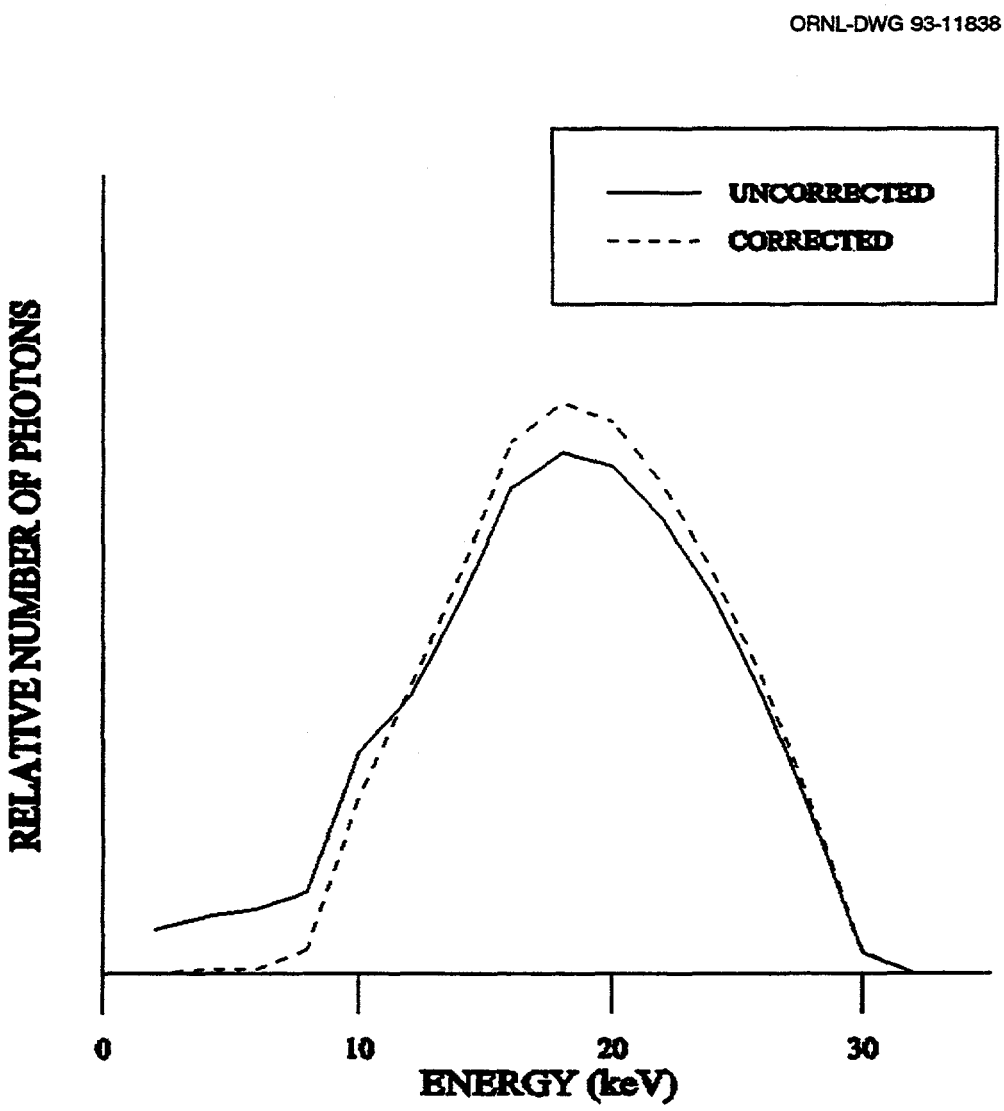

Fig. 4.1. Comparison of a measured "uncorrected" M30 spectrum to a measured corrected M30 spectrum.

5. NEURAL COMPUTING

5.1 DESCRIPTION OF NETWORK

The basic approaches used in neural computing are fundamentally different from those used in conventional computing. Typically an algorithmic or rule-based approach is applied in conventional computing to the input problem in search of a solution. In some instances, the mathematical relationship does not exist or is unclear, and a "nonalgorithmic" process, such as neural computing, is a desirable approach to a solution.[8]

The software package used for this work was NeuralWare NeuralWorks Professional II/Plus. A back propagation network was created with input, hidden, and output layers, which are all interconnected to the succeeding layer. Each processing element or node in the layers carries a weight coefficient, which is determined by presenting the network with a series of input/output pairs. During learning, information is propagated back through the network to adjust the weight coefficients using a learning algorithm. In the case of this error back-propagation network, the learning algorithm is the generalized delta rule. A concise description of this learning algorithm appears in the appendix of the work of Boone et al. (ref. 8). The NeuralWare NeuralWorks software will automatically build a back-propagation network upon the request of the user. The user does, however, have to make some important decisions before requesting the back-propagation network to be built. The number of layers and the number of nodes for each layer must be decided upon, as well as the learning rule, the initial learning coefficients, the transfer function, and whether the network should be hetero- or auto-associative.

By choosing hetero-associative, it signifies that the input is expected to be different from the desired output and that there is an associated output with the entered input training data. The hyperbolic tangent is chosen as the transfer function for this work. The range of the values for the input values is -1.0 to 1.0 and -0.8 to 0.8 for the output values, the default range of *NWorks*. Due to these ranges, equal weight is given to the low and high end values during the multiplication of the output of this function in the weight update equation.[16] The normalized cumulative delta rule is chosen as the learning rule. As a result, the error is reduced by the square root of the number of presentations, tending to prevent large abrupt changes in the weights.[16]

The learning rates were chosen by a process of trial and error and through looking at some descriptions of other networks. According to the manual *Using Nworks*,[16] having a larger learning coefficient at the hidden layer than that for the output layer allows the hidden layer to form "feature detectors" during the initial learning process; these "feature detectors" can contribute to form more complex "detectors" in the output layer. Large learning rates may cause large instabilities preventing convergence.[8]

Figure 5.1 is a diagram of the structure of the neural network. The output layer consists of 16 nodes corresponding to 16 energy bins (0 to 32 by 2 kev) for the M30 spectrum. The use of 16 processing elements in the hidden layer was found to be appropriate for this application. The input layer consists of 160 processing elements that correspond to each of

ORNL-DWG 93-11839

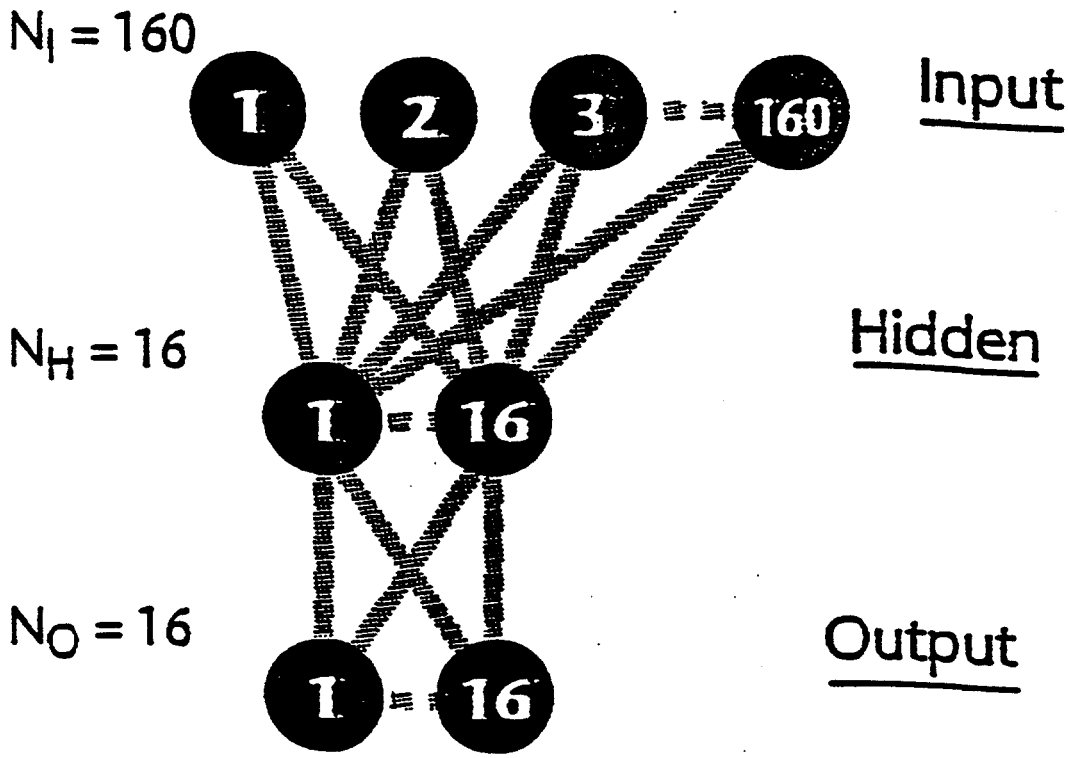

Fig. 5.1. Structure of the M30 neural network showing the three layers and the number of processing nodes in each layer.

16 energy bins for each of ten attenuators. A listing of the attenuators is found in Table 5.1. Since the detector response is dependent on the energy and the amount of attenuation to the X-rays, essentially 160 different detectors were created by using the series of 10 attenuators and analyzing the spectrum in 2 keV energy intervals.

5.2 TRAINING DATA

The optimal training set for the neural network would provide input/output information that covers the domain of interest so the network can find a general solution to a specific problem.[2] Ideally, the training set would be composed of numerous pairs of an unattenuated and attenuated measured spectrum as the input with the corresponding detector-response-matrix-corrected measured spectrum of the beam code under investigation as the output. These spectra would preferably be measurements of the NIST X-ray spectrum, in this case the M30 beam. Since performing these actual measurements at NIST was not feasible, the spectra for the training set had to be obtained with a computational model. Draft ANSI N13.11-1993 contains the new NIST beam codes both in tabular and graphical form as the relative number of photons per keV energy bin. Henceforth, the spectra found in the ANSI standard will be referred to as the base corrected spectra, from which all other training spectra are generated. The base corrected spectrum is the "true" spectrum incident on the detector. The data found in Draft ANSI N13.11-1993 were organized in 2 keV energy intervals for this work.

In the preparation of a broad set of training data it is not necessary to replicate the actual shape of the NIST M30 spectrum. However, the goal of spectral reconstruction, to find the true effect due to attenuation of the spectrum, should be maintained. The generation of many corrected spectra for training the neural network involved making perturbations to the base corrected M30 spectrum; these perturbations are listed in the equations found in Table 5.2. After applying these perturbations to each 2 keV energy interval, the ratio of the sum of the photons in the NIST base corrected spectrum to the sum of the photons in the generated spectrum was found and then multiplied by sum of photons in each interval of the generated spectrum. This normalization was applied to all of the generated spectra. The generated spectra are the output portion of the training set and are referred to as the corrected spectra.

Voltage oscillations were present especially in the measurements that required a longer counting time. Since a calibrated voltage stabilizer was not available, there was no way to correct for these experimentally. In an attempt to generate realistic data that simulated these voltage changes, slight changes were made to the energy range of these perturbed spectra. The energy range was changed by 1.05, 1.025, and 0.975, covering a new maximum energy range of 29.25 to 31.5 keV. The effect on the NIST base corrected spectrum is expressed graphically in Fig. 5.2. The NIST base corrected spectrum was fit to these altered energy scales using a curve fitting routine offered in the Grapher software package by Golden Software. These three "new" base corrected spectra were then perturbed using the first eleven equations found in Table 5.2 and normalized as described above. These 54 corrected spectra comprise the output portion of the training set and are shown graphically in Figs. 5.3, 5.4, and 5.5.

Table 5.1. Aluminum attenuators used for the neural network spectral analysis (The attenuators are in addition to the base filtration)

Attenuator ID number	M30 (mm)
1	0.0
2	0.020
3	0.031
4	0.049
5	0.095
6	0.184
7	0.519
8	5.084
9	9.950
10	20.086

Table 5.2. Spectra used for the training of the neural network

Spectrum identification number	Equation of training spectra E = energy interval B = base NIST spectrum
1	Y = B
2	Y = B*E
3	Y = B/E
4	Y = B*exp(–0.01*E)
5	Y = B*exp(0.01*E)
6	Y = B/(exp(0.02*E)-exp(0.01*E))
7	Y = B*(exp(0.02*E)-exp(0.01*E))
8	Y = B*exp(-0.02*E)
9	Y = B*exp(0.02*E)
10	Y = B/(exp(0.03*E)-exp(0.005*E))
11	Y = B*(exp(0.03*E)-exp(0.005*E))
12	Y = B*exp(-0.005*E)
13	Y = B*exp(0.005*E)
14	Y = B/(exp(0.03*E)-exp(0.01*E))
15	Y = B*(exp(0.03*E)-exp(0.01*E))
16	Y = B*exp(-0.03*E)
17	Y = B*exp(0.03*E)
18	Y = B/(exp(0.01*E)-exp(0.005*E))
19	Y = B*(exp(0.01*E)-exp(0.005*E))
20	Y = B*exp(-0.04*E)
21	Y = B*exp(0.04*E)
22–32	Variation of spectra 1–11 (fit of base spectrum for E*1.05)
33–43	Variation of spectra 1–11 (fit of base spectrum for E*1.025)
44–54	Variation of spectra 1–11 (fit of base spectrum for E*0.975)

ORNL-DWG 93-11840

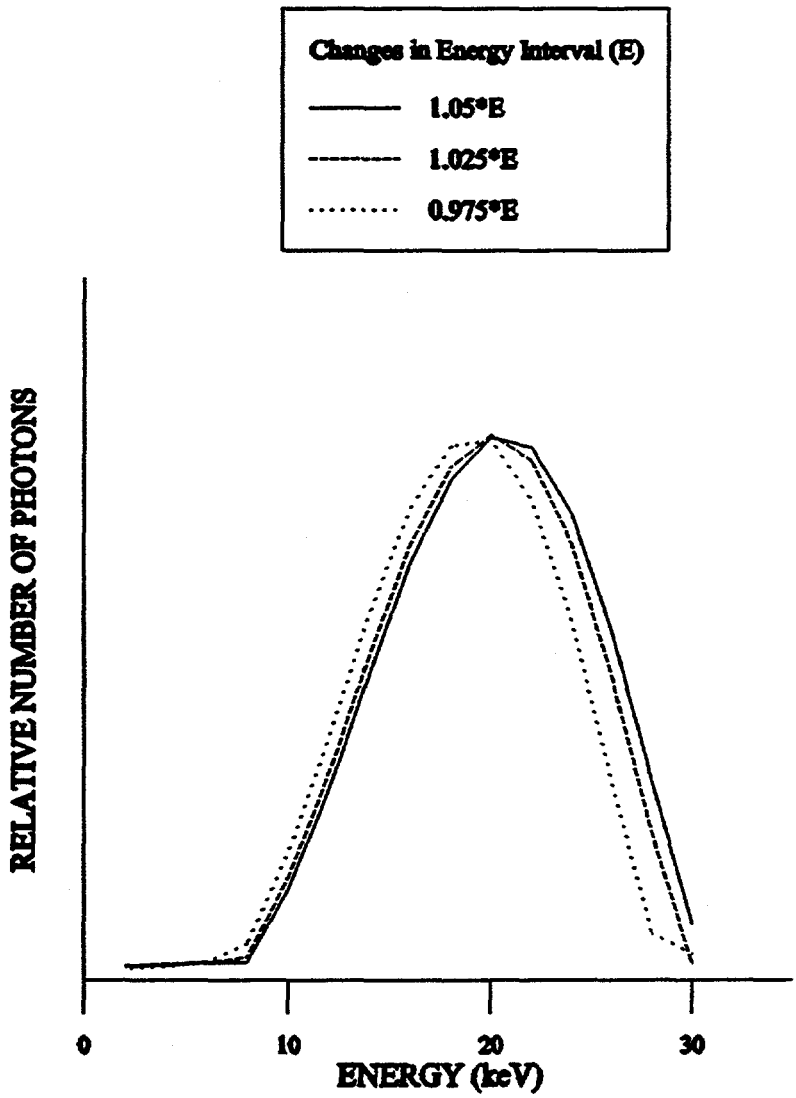

Fig. 5.2. Base spectra used to generate additional spectra with an altered energy range for the training of the M30 neural network.

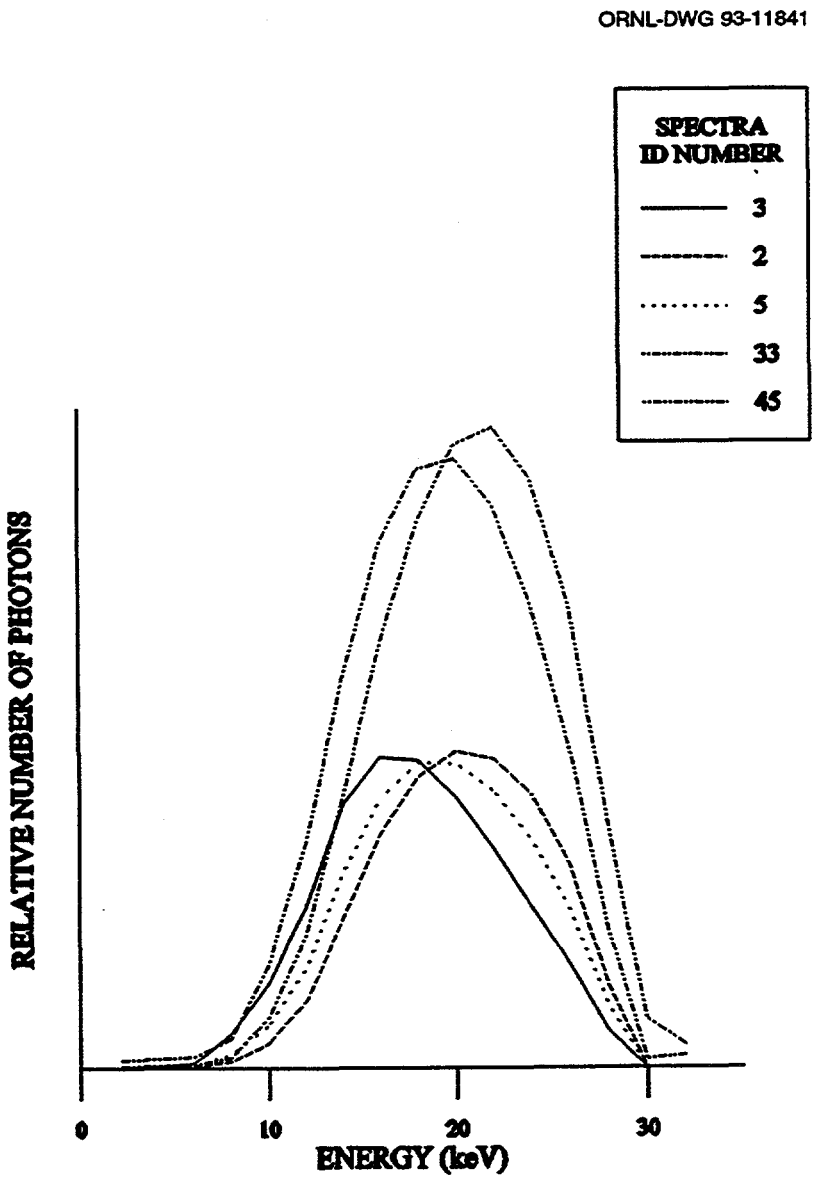

Fig. 5.3. First set of examples of some generated spectra used in the training of the neural network.

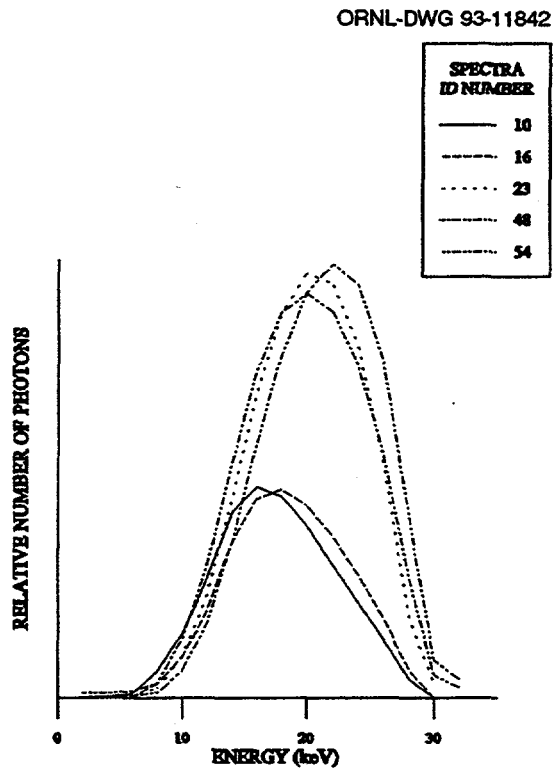

Fig. 5.4. Second set of examples of some generated spectra used in the training of the neural network.

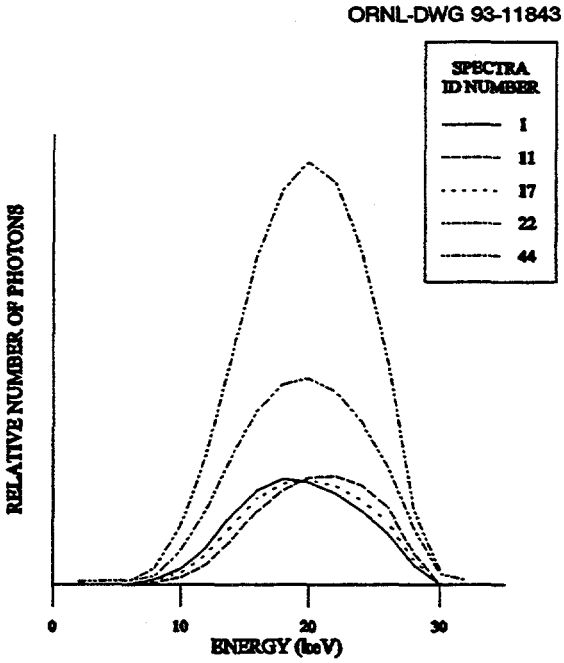

Fig. 5.5. Third set of examples of some generated spectra used in the training of the neural network.

Preparation of the input portion of the training set was a much more complex process than that for the output portion. As mentioned previously, the input is analogous to 10 measured spectra, 1 unattenuated and 9 attenuated, with the designated attenuators. Therefore, for every output training spectrum there are 10 associated input spectra. These 10 input spectra were calculated for each of the 54 corrected output spectra. In each case, the output spectrum was attenuated by each of the Al attenuators listed in Table 5.1, resulting in one unattenuated corrected spectrum and nine attenuated corrected spectra. A graph of these attenuations to the NIST base corrected spectrum is found in Fig. 5.6.

The next step in the input preparation process is to "un-correct" these detector-response-matrix-corrected spectra to obtain spectra equivalent to raw MCA data. In essence, the detector response had to be calculated out of the corrected spectra. This was accomplished with a modified backstripping response matrix code, which is explained in Sect. 5 and in detail in Appendix B. This modified code permitted the corrections made to the initial MCA data to be eliminated (i.e., reversed), resulting in spectra characteristic of raw MCA data.

The changes to the backstripping code were tested on MCA data for X-ray beams ranging in energy from 30 keV to 100 keV provided by the FDA. Figure 5.7 shows an example of this "un-correction" process, in which the modified code has been applied to the NIST M30. All 54 corrected spectra and the associated attenuated spectra were organized into the necessary format of input/output pairs as required by the NeuralWare software package.

ORNL-DWG 93-11844

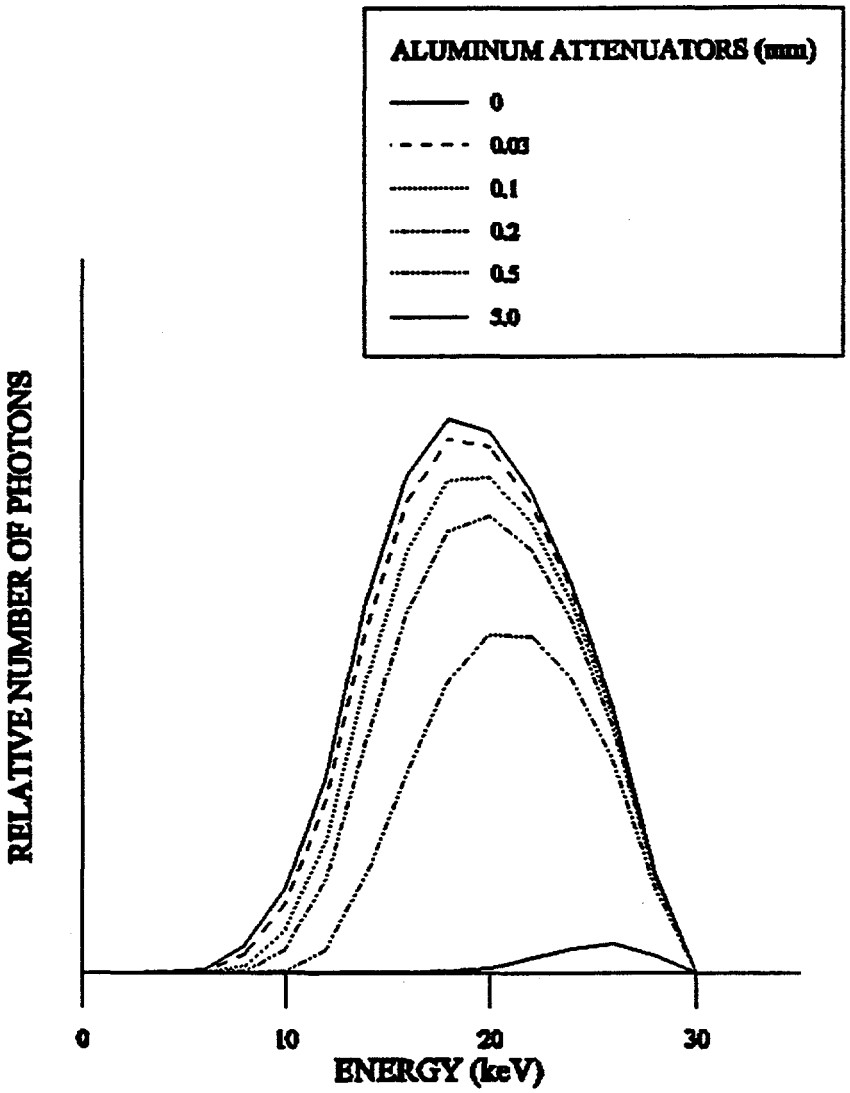

Fig. 5.6. The NIST M30 beam attenuated with the series of attenuators.

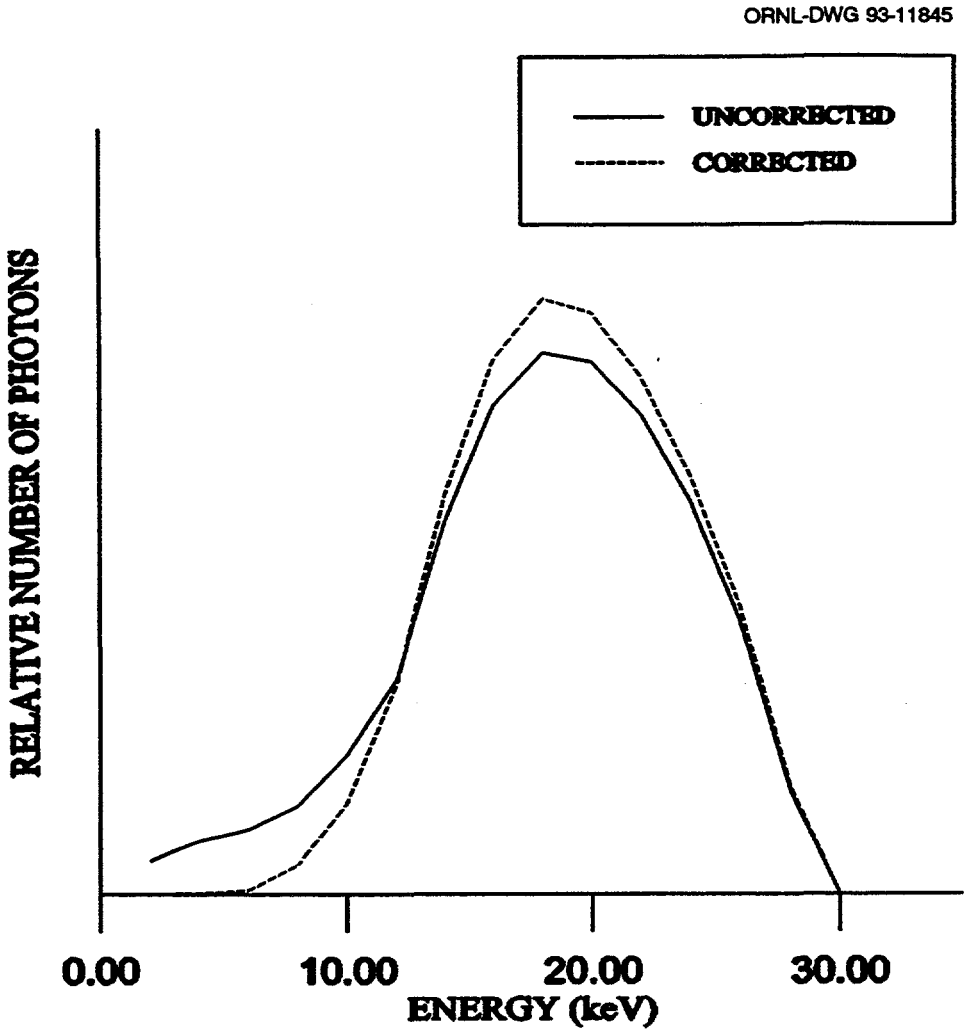

Fig. 5.7. Comparison of the NIST M30 to an "uncorrected" spectrum.

5.3 NORMALIZATION

The input/output training data must be scaled for the chosen neuro-dynamic transfer function. In the case of this M30 network, which has an hyperbolic tangent transfer function at the output layer, all output data must be between -0.8 and 0.8 The *NWorks* software package has a simple preprocessing facility available. A brief description of this scaling process follows, with a more detailed description following in Appendix A. The pre-processing facility of *NWorks* determines the maximum and minimum values for each data field for all the input and output data files. The data fields for this network correspond to the 16 energy intervals. The maximum and minimum values are then stored to a table called the MinMax table. The range to which the input and output data must be scaled is dependent on the transfer function chosen. As part of the testing/recall feature of *NWorks*, the result of the network is "de-scaled" to realistic values.[16]

The M30 neural network was trained on 50 of the 54 input/output training sets. The remaining four training sets were used for testing the trained network since they contained data never before entered into the network. After 150,000 to 300,000 iterations, the network converged at a tolerance of 0.02 for the root mean square error for all processing nodes in the output layer. After this convergence the four remaining training sets were successfully tested in the network, and the root mean square errors were all less than 0.02.

Spectral measurements were made on the M30 beam using the same set of attenuators (Table 5.2) used in calculating the training data. Some of these attenuated M30 spectra can be found graphically in Figs. 5.8 and 5.9. The ratio of the sum of the photons in the NIST base corrected spectrum to the sum of the photons in the measured spectrum was found and then multiplied by each 2 keV interval of the measured spectrum. This normalization was accomplished for each of the 10 measured spectra. After the data were organized in the necessary format for the *Nworks* software, they were scaled using the MinMax option of *NWorks*. The recall option of this software was then used to obtain the corrected spectrum resulting from the input measured data. Results follow in Sect. 6.

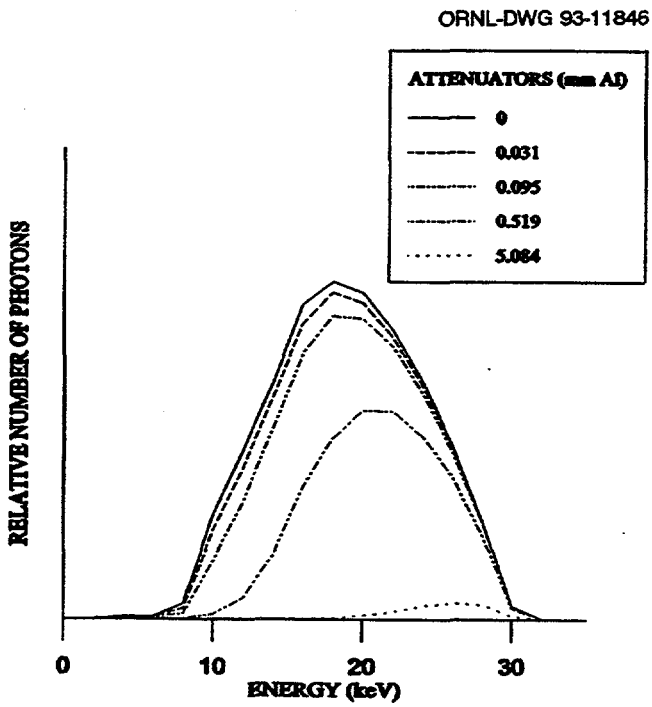

Fig. 5.8. The measured M30 spectrum attenuated with five different attenuators.

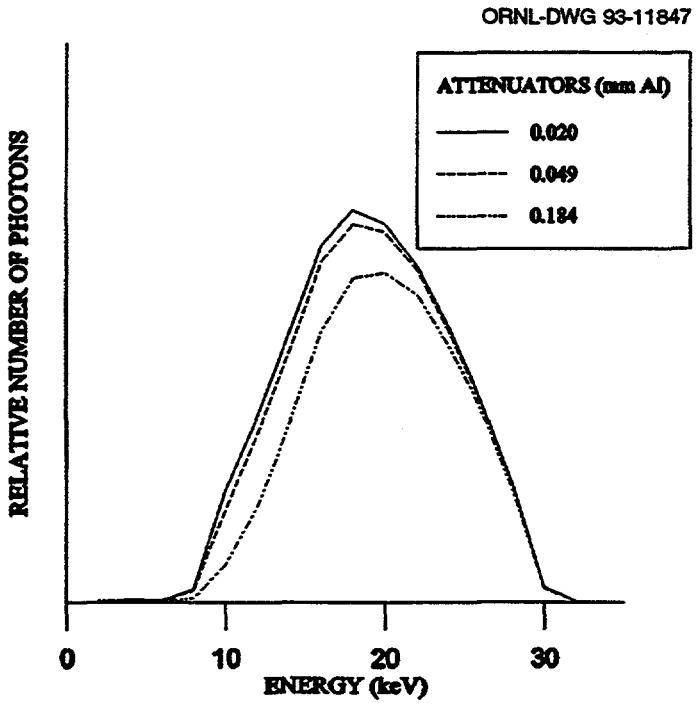

Fig. 5.9. The measured M30 spectrum attenuated with three different attenuators.

6. RESULTS AND COMPARISON OF SPECTRAL ANALYSIS

A reconstruction technique that determines the attenuation of the spectrum with minimal error would be the spectral analysis of choice. In comparing the resulting spectra from the response matrix correction procedure and from the neural network to the ideal NIST spectrum, differences can be found in both the low and the high energy portions of the spectra (see Fig. 6.1). Figure 6.2 emphasizes that the response matrix correction procedure adds error to the low energy portion of the spectrum, indicating more attenuation is needed in order to have the RADCAL M30 match the NIST M30 beam. The neural network M30 spectrum illustrates the excess of attenuation. Ideally, all of the M30 spectra in Fig. 6.1 should match exactly at the upper energy portion. Since the match is not exact with either correction technique, it is expected that voltage inconsistencies occurred while collecting the spectral data. The use of a voltage divider would help to diminish voltage inconsistency. In preparing the neural network training data, this voltage inconsistency problem was addressed by attempting to generate training data that were in a range above and below the nominal kilovoltage setting. More training data reflecting these voltage fluctuations would improve the network results.

An evaluation of the best match of an attenuated M30 spectrum to the NIST M30 can be made by examining the results of the response matrix correction technique. Figure 6.3 shows the attenuation of the M30 beam with 0.03 mm Al, and Fig. 6.4 shows the best match of an attenuated spectrum with 0.01 mm Al. An additional thickness of 0.01 mm Al could be added to the base filtration of the M30 beam and additional spectral measurements could be made using the designated set of attenuators. These data could then be entered into the neural network as before. The expected result would be an overly attenuated spectrum, according to the response matrix correction technique results.

The ideal test for the M30 neural network would be to have the opportunity to actually take numerous measurements of the NIST M30 spectrum using the equipment of the RADCAL facility, the identical set-up, and the same set of attenuators in the study. These data would be used to train the network in the same manner as described in Sect. 2.

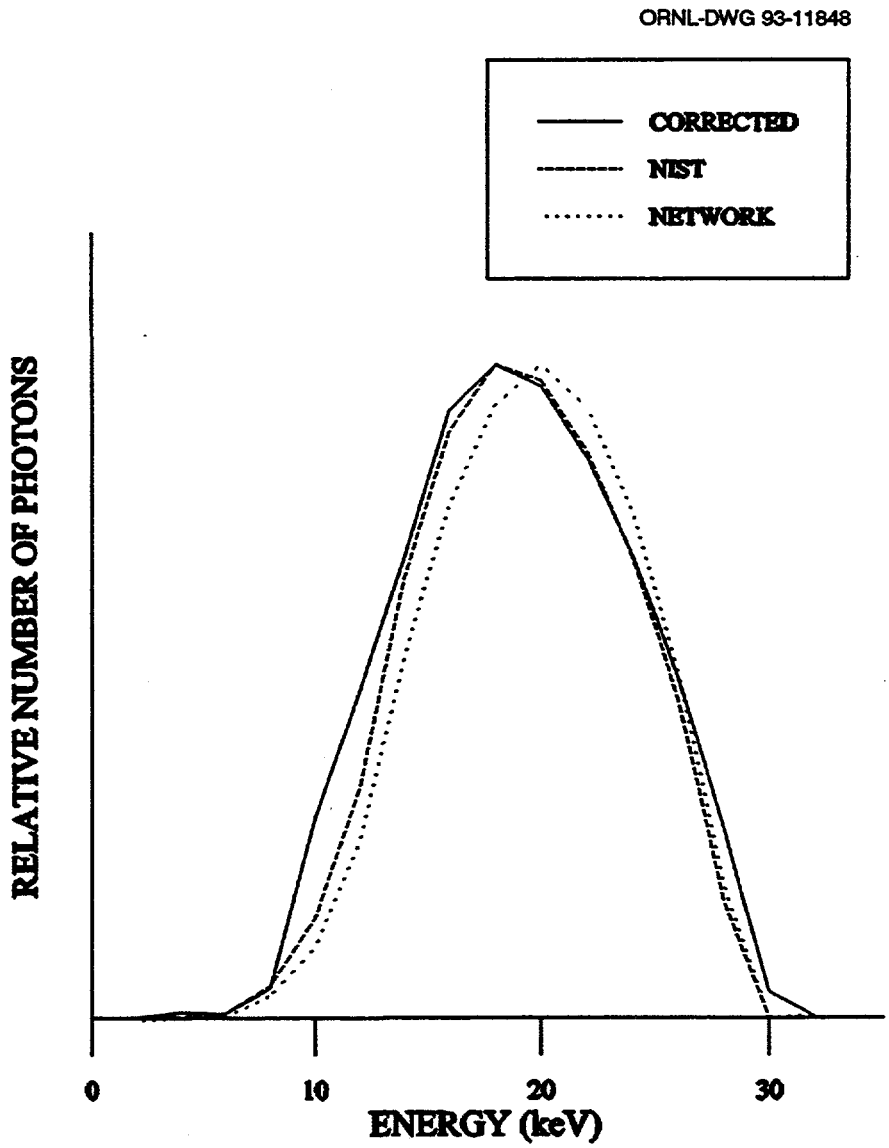

Fig. 6.1. Comparison of the M30 network spectrum to the M30 NIST and M30 measured spectra.

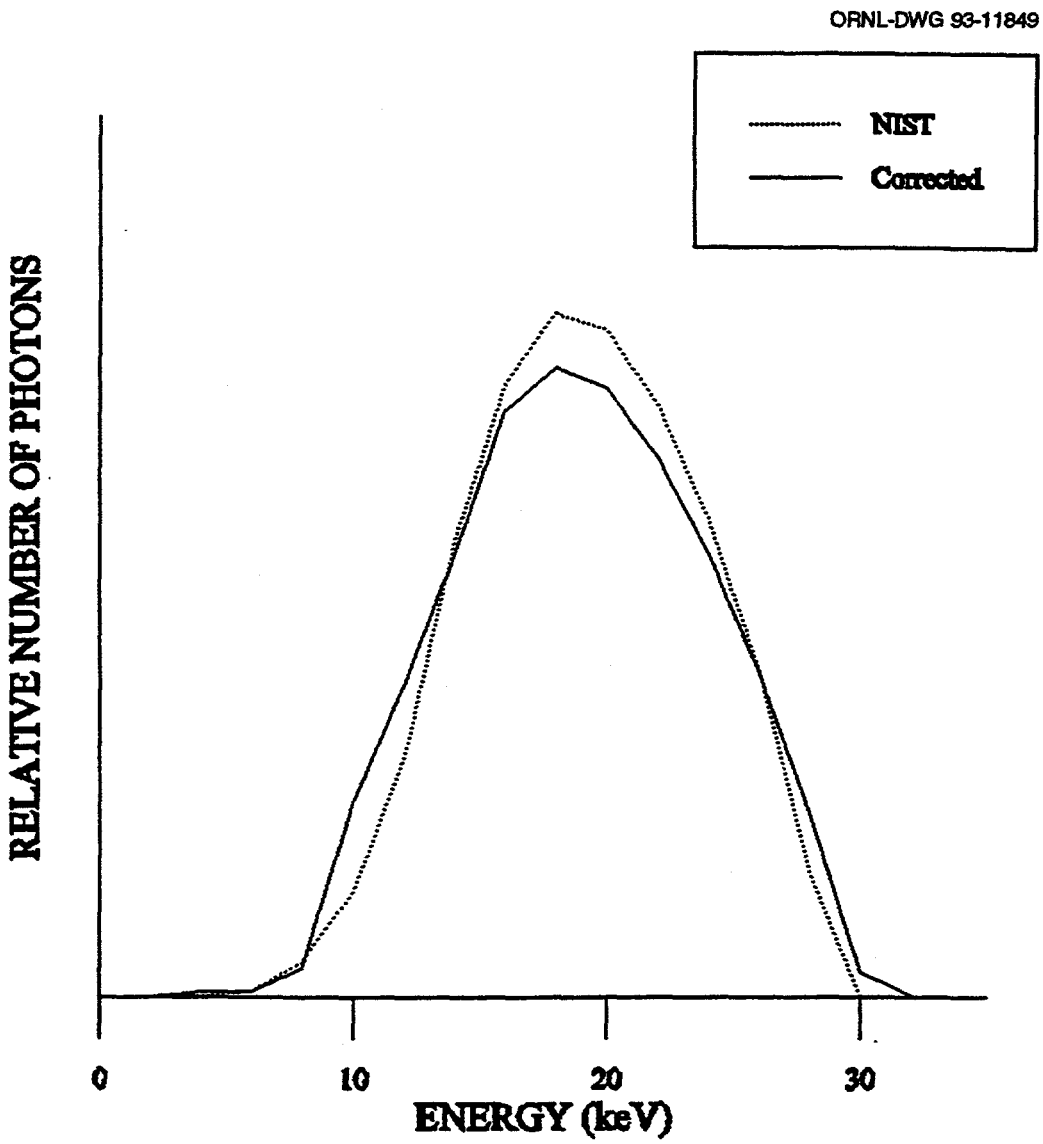

Fig. 6.2. Comparison of the NIST M30 spectrum to the response matrix corrected M30 spectrum.

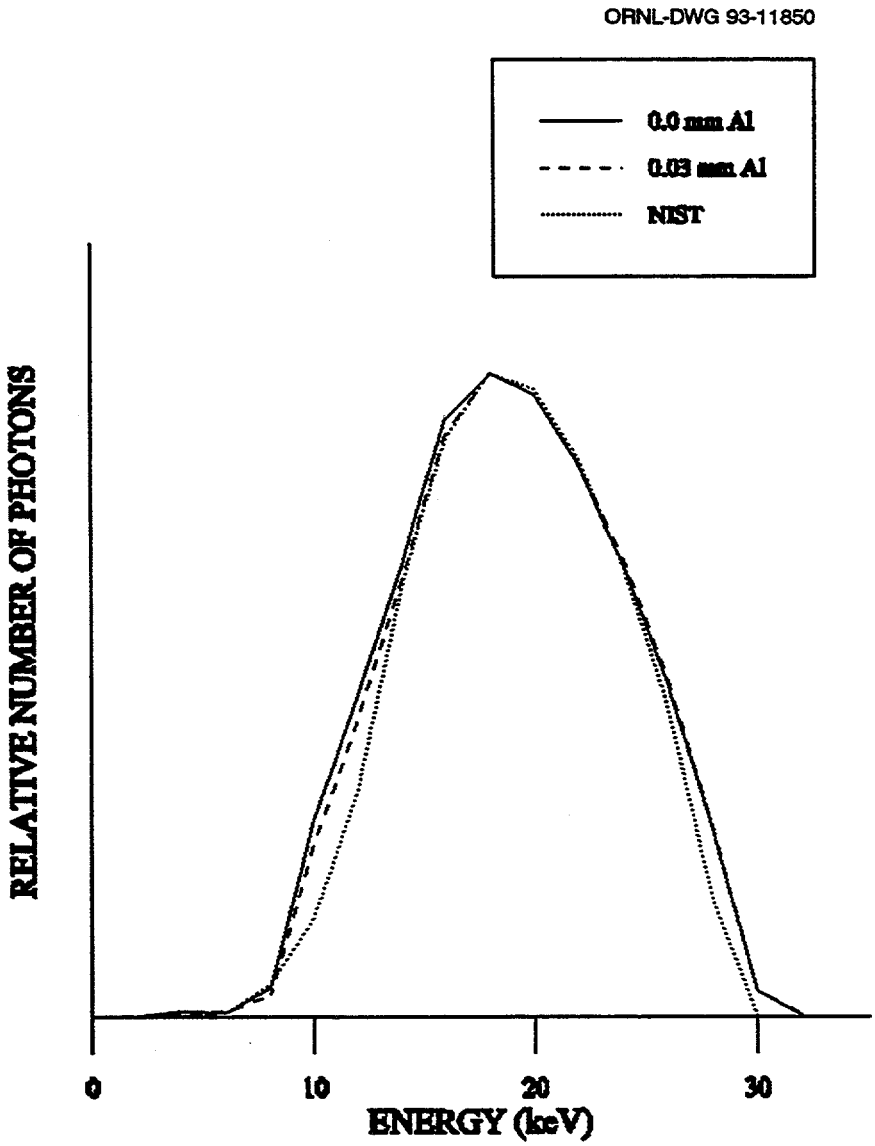

Fig. 6.3. Comparison of M30 NIST spectrum to two measured corrected attenuated M30 spectra.

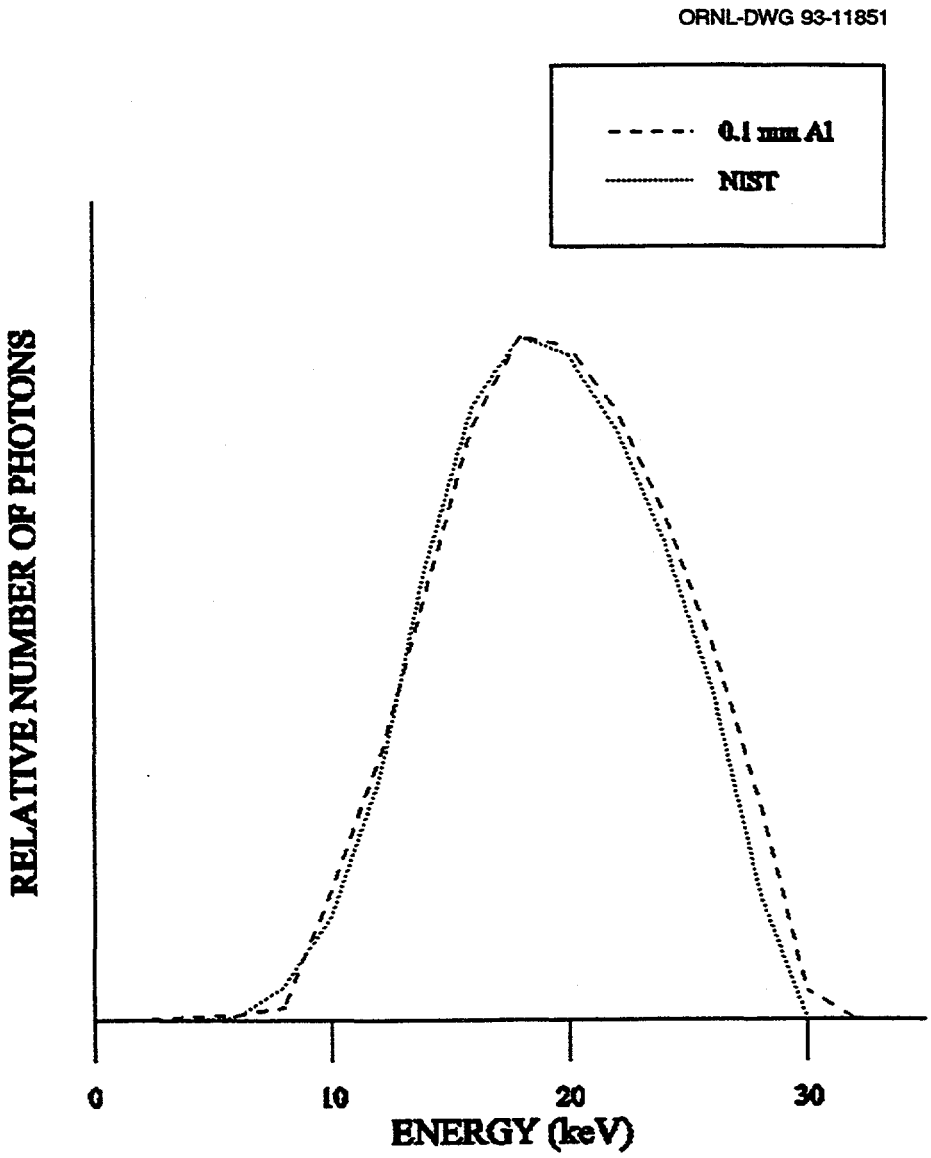

Fig. 6.4. The best match of an attenuated measured spectrum to the NIST M30 spectrum.

7. CONCLUSIONS

The process of calibrating an X-ray beam and determining the X-ray beam quality involves fairly straightforward techniques. The calibration can be achieved through obtaining a series of attenuation measurements, making the proper corrections, and determining the HVL and HC. This process was successfully completed for five of the NIST beam codes. The X-ray beams have been used to make calibrated exposures to personnel dosimeters for routine calibration checks and for making exposures in the 1993 Personnel Dosimeter Intercomparison Study.

The spectral reconstruction techniques investigated in this work are not straightforward processes. Performing a complete and detailed investigation of the error and the uncertainty involved with the various spectral analyses would be a complex process and is beyond the scope of this work. However, it is interesting to note the obvious uncertainties involved with the different approaches to a spectral analysis. Many of the spectral analysis techniques, although not fully investigated in this work, use attenuation measurements to reconstruct the spectra. As the attenuation to the X-ray beam is increased, a proportionately larger number of lower energy X-rays are attenuated out of the spectrum. Larger increases in the thickness of the attenuators also decrease the number of higher energy photons that are transmitted. The effect of the attenuation on the change in the number of higher energy photons transmitted is less than the change for the lower energy photons. The decrease in the change of the number of photons collected with increasing thickness leads to an increased uncertainty associated with the higher energy portion of the spectrum.

If one is fortunate to have an appropriate high-purity germanium spectroscopy system, a complete spectrum can be obtained with minimal work. Before any detector interactions are considered, the uncertainty involved in the MCA data is strictly a function of the number of counts in the energy bins. Since the maximum number of counts is collected in the bin that corresponds to the effective energy of the spectrum, the relative uncertainty (coefficient of variation) would be at a minimum at this point. The upper one third of the spectrum, which is the portion of the spectrum with the highest number of photons, would certainly have a lower relative uncertainty than the lower energy portion of the spectrum where fewer counts are collected. The relative uncertainty would also be higher for the extreme high end of the spectrum where fewer photons are collected. If one attempts a backstripping procedure on the MCA data obtained through the spectroscopy system, the uncertainty is not just a function of the number of counts in the energy interval but is also a result of the backstripping procedure. Since the backstripping procedure first corrects the counts in the higher energy portion of the spectrum and then superimposes the probable corrected number of counts to the lower energy intervals, the uncertainty is higher at the lower portion of the spectrum.

The uncertainty involved with the reconstructed spectrum resulting from the neural network is really a combination of uncertainties from detection, backstripping, and from all the uncertainties in the neural analysis itself. The uncertainty is lower in the lower portion of the spectrum for the network spectrum than from the response matrix backstripped spectrum. The uncertainty that is involved with the higher energy portion of the network

spectrum results from the lack of training data that properly represents the voltage fluctuations. With further work and additional training data, this spectral analysis technique has the potential to become a technique that has a lower associated uncertainty.

REFERENCES

1. *American National Standard for Dosimetry—Personnel Dosimetry Performance—Criteria for Testing*, ANSI N13.11-1993, American National Standards Institute, Inc., New York, 1993 (Draft).

2. J. M. Boone, "X-Ray Spectral Reconstruction from Attenuation Data Using Neural Networks," *Med. Phys.* 17, 647–654 (1990).

3. R. E. Lapp and H. L. Andrews, *Nuclear Radiation Physics*, 3rd ed., Prentice-Hall, Inc., Englewood Cliffs, New Jersey, 1964.

4. S. C. Bushong, *Radiologic Science for Technologists*, 4th ed., C. V. Mosby Company, St. Louis, Missouri, 1988.

5. P. J. Lamperti, T. P. Loftus, and R. Loevinger, *Calibration of X-Ray and Gamma-Ray Measuring Instruments*, National Bureau of Standards spec. publ. 250–16, U.S. Government Printing Office, Washington, D.C., 1988.

6. B. R. Archer and L. K. Wagner, "A Laplace Transform Pair Model for Spectral Reconstruction," *Med. Phys.* 9, 844–847 (1982).

7. P. H. Huang, T. S. Chen, and K. R. Kase, "Reconstruction of Diagnostic X-Ray Spectra by Numerical Analysis of Transmission Data," *Med. Phys.* 15, 707–710 (1986).

8. J. M. Boone, V. G. Sigillito, and G. S. Shaber, "Neural Networks in Radiology: An Introduction and Evaluation in a Signal Detection Task," *Med. Phys.* 17, 234–241 (1990).

9. H. T. Heaton, *Secondary-Level Laboratories: Methodology for a Calibration Program*, unpublished, private communication from H. T. Heaton, National Institute of Standards and Technology, 1993.

10. B. R. Archer and L. K. Wagner, "Determination of Diagnostic X-Ray Spectra with Characteristic Radiation Using Attenuation Analysis," *Med. Phys.* 15, 637-641 (1988).

11. E. H. Eisenhower, *Criteria for the Operation of Federally-Owned Secondary Calibration Laboratories (Ionizing Radiation)*," National Institute of Standards and Technology spec. publ. 812, U.S. Government Printing Office, Washington, D.C., 1991.

12. S. M. Seltzer, "Calculated Response of Intrinsic Germanium Detectors to Narrow Beams of Photons with Energies up to ~300 keV," *Nucl. Instrum. Methods*, 188, 133-151 (1981).

13. H.-P. Chan, C.-T. Chen, K. Doi, T. R. Fewell, and R. E. Shuping, "Investigation of Energy Responses of Germanium Detectors and Correction of Measured Spectra by Means of Monte Carlo Simulation," *Rad. Res.*, 99, 443-464 (1984).

14. C. S. Chen, K. Doi, C. Vyborny, H.-P. Chan, and G. Holje, "Monte Carlo Simulation Studies of Detectors Used in the Measurements of Diagnostic X-Ray Spectra," *Med. Phys.* 7, 627-635 (1980).

15. T. R. Fewell, R. E. Shuping, and K. R. Hawkins, *Handbook of Computed Tomography X-Ray Spectra*, HHS Publication (FDA) 81-8162, Public Health Service Food and Drug Administration, U.S. Department of Health and Human Services, Rockville, Maryland, 1981.

16. NeuralWare, *NeuralWorks Professional II/Plus* and *NeuralWorks Explorer*, 1991.

Appendix A

DESCRIPTION OF MINMAX SCALING

The information in the following description is taken from the *Reference Guide* of the NeuralWare Software package. The MinMax table is a utility (offered by *NWorks*) that automatically scales the I/O data into acceptable specified ranges for the network. The MinMax table is also used to descale the network values to values for the output. Note that the MinMax data reside in a file referred to as a set of records, where each record consists of a set of numeric fields.

In a hetero-associative network, each presentation of data is represented by a data record consisting of a set of I input fields followed by a set of D desired output fields, where I and D are the number of input and output processing elements in the network:

$$f_1 f_2 \ldots f_I f_{I+1} \ldots f_{I+D} \; . \tag{A-1}$$

A MinMax table consists of two sets of values

$$m_1 m_2 \ldots m_I m_{I+1} \ldots m_{I+D} \; , \tag{A-2}$$

and

$$M_1 M_2 \ldots M_I M_{I+1} \ldots M_{I+D} \; , \tag{A-3}$$

with indices corresponding to those of the data record. For a given index k, m_k and M_k correspond to the minimum and maximum value respectively that f_k could have. The minimum and maximum (m_k and M_k) represent the range for the linear mapping from data field to network processing element. The input and output ranges can be denoted by (r_I, R_I) and (r_D, R_D). Let i_j be the network input corresponding to the real world value f_j, let d_k be the network desired output corresponding to the real world value f_k, let o_k be an actual network output, and let g_k be the corresponding real world output. The mappings from the real world to the network are as follows.
Input:

$$i_j = \frac{(R_I - r_I) * f_j + (M_j * r_I - m_j * R_I)}{(M_j - m_j)} \; ; \tag{A-4}$$

Desired output:

$$d_k = \frac{(R_D - r_D) * f_k + (M_K * r_D - m_k * R_D)}{(M_k - m_k)} \; . \tag{A-5}$$

On output, the mapping from network output to real world is

$$g_k = \frac{(M_k - m_k) * o_k + (R_D * m_k - r_D * M_k)}{(R_D - r_D)} \quad . \qquad \text{(A-6)}$$

Non-numeric fields and missing fields are mapped to the middle of the target range ($0.5 * (R_I + r_I)$ or $0.5 * (R_D + r_D)$).

Appendix B

BACKSTRIPPING

The following information was taken in part from the appendix of Chan et al. (ref. 13).

In order to use the following spectrum correction procedure the energy resolution of the X-ray detector needs to be narrower than the energy interval used in the response matrix. The Monte Carlo data are converted from percentage values to fractional values and then used to create a triangular response matrix R for the HPGe. Each row of R, identified by the subscript i, represents the detector's response to a monoenergetic photon energy. Each column value, identified by a subscript j, tabulates the probability of detecting the monoenergetic photon in each 2-keV interval, centered on the even 2-keV values. Since the detector resolution is smaller than the 2-keV interval, the diagonal values of R are also equivalent to the photopeak efficiency of the detector for each monoenergetic photon energy. In summary, a matrix element R_{ij} tabulates the probability that an incident monoenergetic photon of energy E = 2i keV is detected in the energy interval between (2j - 1) and (2j + 1)keV; therefore, R_{ij} is equal to the photopeak efficiency at E for i = j and is zero for i < j.

A matrix A is formed that is compatible with R from the experimental spectrum's pulse height distribution. The experimental data are summed and reduced into 2-keV intervals, which are identified by the subscript n. The energy interval determines the value of n (which is the same value as the row indicator i) of R so n = i = E/2. In the development of these matrices the 0 to 1 keV interval has been ignored to simplify formulating the triangular response matrix. Since there are no data in this interval, the final results are not affected.

The correction procedure uses R to perform a step-by-step procedure on the experimental data. The correction starts with the highest energy interval, A_k, where k is equal to the maximum value of n and is given by $n_{max} = k = E_{max}/2$. All counts in this interval result from the photopeak efficiency of the detector since there is no contribution from the K escape or Compton interactions at this high energy. The true count, T, in the kth interval T_k can be calculated as

$$T_k = \frac{A_k}{R_{kk}}, \qquad \text{(B-1)}$$

where R_{kk} is the diagonal matrix value, which has already been shown to be equivalent to the photopeak efficiency and occurs when k = i = j. The T_k can be combined with the other values in the kth matrix row to calculate and strip out the counts that this interval has contributed to all of the lower energy intervals. This is accomplished by means of the iteration procedure

$$A_n = A_n - (T_k)(R_{kj}), \qquad \text{(B-2)}$$

where the n and j indicators are equal and are varied simultaneously from 1 to k - 1 (k is held constant for this). Upon the completion of this procedure a matrix A results that has been corrected for Compton and K escape interactions. The lower energies of this new pulse height distribution can now be corrected by applying a similar procedure: the i and n values are reduced to k - 1, and then the above operations are repeated. This procedure is repeated until each A_n value has been replaced by a T value.[13]

Appendix C

DESCRIPTION OF TOM HEATON'S HVL CODE

This information was taken in part from an unpublished manual by Tom Heaton. The portion related to this work is included here.

The computer code assumes that the measured calibration factors were fit with the functional form, which relates the calibration factors to the HVL. The relationship of the calibration factors for an A-3 ion chamber as a function of the HVL value is described by equation C-1,

$$CF = b_o + b_1 \ln(HVL) + b_2 \ln^2(HVL) + b_3 \ln^3(HVL) , \qquad \text{(C-1)}$$

where the coefficients have the following values:

$b_o = 1.036364$, $b_2 = 0.0338613$,
$b_1 = -0.066577$, $b_3 = -0.00395484$.

The following calculations are performed to determine the HVL for a given filter thickness.

1. The transmission curve (T), which is found by attenuating the X-ray beam with a series of Al filters, is measured to at least the tenth value layer. A cubic polynomial regression analysis is made between the added filter material (l) and the log of transmission to determine the coefficients β_o, β_1, β_2, and β_3

$$l = \beta_o + \beta_1 \ln T + \beta_2 \ln^2 T + \beta_3 \ln^3 T . \qquad \text{(C-2)}$$

It is assumed that the same value of β_o, β_1, β_2, and β_3 can be used to determine the transmission curve (T) when l is known

$$T = e^{-f(\beta_o, \beta_1, \beta_2, \beta_3, l)} , \qquad \text{(C-3)}$$

where

$$f(\beta_0, \beta_1, \beta_2, \beta_3, l) = 2\sqrt{-\frac{A}{3}} \cos\left[\frac{1}{3}\cos^{-1} u + \frac{n\pi}{3}\right] - \frac{\beta_2}{3\beta_3} , \qquad \text{(C-4)}$$

and where the variables A, B, and u are described by equations C-5, C-6, and C-7.

$$A = \frac{(3\beta_1\beta_3 - \beta_2^3)}{3\beta_3^2} , \qquad \text{(C-5)}$$

$$B = \frac{(2\beta_2^3 - 9\beta_1\beta_2\beta_3 + 27(\beta_o - l)\beta_3^2)}{27\beta_3^3} , \qquad \text{(C-6)}$$

2. For each point with added thickness l_i calculate the half transmission of Al or Cu at the half transmission of the point $T_{\frac{1}{2}}(i)$ by

$$T_{½}(i) = \frac{1}{2}\exp[-f(\beta_o, \beta_1, \beta_2, \beta_3, l_i)] \; . \qquad \text{(C-8)}$$

3. Use this value of $T_{½}(i)$ to determine the total added thickness of Al or Cu at the half value of the measured point by

$$l_{½}(i) = \beta_o + \beta_1 \ln T_{½}(i) + \beta_2 \ln^2 T_{½}(i) + \beta_3 \ln^3 T_{½}(i) \; . \qquad \text{(C-9)}$$

4. The half-value layer for point i is

$$HVL(i) = l_{½}(i) - l(i) \; . \qquad \text{(C-10)}$$

5. Using the relationship of the calibration factors to HVL and the coefficients from above, calculate the correction factor for point i from

$$CF(i) = b_o + b_1 \ln HVL(i) + b_2 \ln^2 HVL(i) \; . \qquad \text{(C-11)}$$

6. To determine a new transmission curve use a "base" function for the i measured points

$$T'(i) = \frac{CF(i) \bullet Base(i)}{CF(o) \bullet Base(o)} \; . \qquad \text{(C-12)}$$

The base can be either the original raw data or the fit function using the original β_o, β_1, β_2, and β_3 values. The index o means no added Al point.

7. Fit the iterated data with a cubic polynomial to determine a new β'_o, β'_1, β'_2, and β'_3 and

$$l' = \beta'_o + \beta'_1 \ln T' + \beta'_2 \ln^2 T' + \beta'_3 \ln^3 T' \; . \qquad \text{(C-13)}$$

The process is repeated to step 4.

8. Stop after the chosen number of iterations, three for this work.
For $\beta'_o = 0$ let β'_1, β'_2, and β'_3 be defined as B, C and D in the following equation

$$l = \beta_o + \beta_1 \ln T + \beta_2 \ln^2 T + \beta_3 \ln^3 T \; , \qquad \text{(C-14)}$$

so the following equation results

$$l = B \ln T + C \ln^2 T + D \ln^3 T \; . \qquad \text{(C-15)}$$

The X-ray beam is generally characterized in terms of HVL and HC. For most beams, D/C < 0.1 and is typically zero within the statistical uncertainty of the fit so one could reanalyze the transmission data with only one term up to $\ln^2 T$. In this case one can make a one-to-one correspondence between (B, C) and (HVL, HC) using the following equation

$$l = B \ln T + C \ln^2 T \; , \qquad \text{(C-16)}$$

then

$$HVL = \ln(0.5)\, B + \ln^2(0.5)\, C = -\ln(2)\, B + \ln^2(2)\, C \; , \qquad \text{(C-17)}$$

$$QVL = \ln(0.25) B + \ln^2(0.25)\, C = -2\ln(2)\, B + \ln^2(2)\, C \; , \qquad \text{(C-18)}$$

$$HC = \frac{HVL}{QVL - HVL} = \frac{1 - C \bullet \ln(2)/B}{1 - 3C \bullet \ln(2)/B}, \quad \text{(C-19)}$$

so

$$B = \frac{HVL \bullet [1/HC - 3]}{2\ln(2)} = \frac{(QVL - 4HVL)}{2\ln(2)}, \quad \text{(C-20)}$$

$$C = \frac{HVL \bullet [1/HC - 1]}{2\ln^2(2)} = \frac{(QVL - 2HVL)}{2\ln^2(2)}. \quad \text{(C-21)}$$

For the more general case with $D \neq 0$ one needs three parameters such as half-, quarter-, and eight-value layers. The corresponding equations are

$$l = B \bullet \ln(T) + C \bullet \ln^2(T) + D \bullet \ln^3(T), \quad \text{(C-22)}$$

and

$$B = \frac{(9QVL - 18HVL - 2EVL)}{6\ln(2)}, \quad \text{(C-23)}$$

$$C = \frac{(4QVL - 5HVL - EVL)}{2\ln^2(2)}, \quad \text{(C-24)}$$

$$D = \frac{(3QVL - 3HVL - EVL)}{6\ln^3(2)}. \quad \text{(C-25)}$$

In the final linear regression iteration between the added Al and log of transmission, the value for zero added filter material should be unity to within the calculated uncertainty if all the measurements are correct. Likewise, the coefficient β_0 in the following equation

$$l = \beta_o + \beta_1 lnT + \beta_2 \ln^2 T + \beta_3 \ln^3 T, \quad \text{(C-26)}$$

should be zero to within its calculated uncertainty. The coefficient β_1 corresponds to $-1/\mu$ or the reciprocal of the attenuation coefficient.

The code can be used to start the calculations with zero added Al or the user can select a different starting point on the transmission curve and subtract the amount of Al at that point from the rest of the values of added Al. For each of the starting points a "new" base filter pack is effectively created, and the code calculates the HVL and HC for that beam. Based on these values, it also calculates the corresponding B and C, resulting in the HVL for several base filters from only one measurement. Due to the length of the code it is not included in this work.

DISTRIBUTION

1. A. B. Ahmed
2. B. A. Berven
3. J. S. Bogard
4. M. A. Buckner
5. L. F. Miller
6. M. L. Souleyrette
7. R. E. Swaja
8. Central Research Library
9. ORNL Technical Library, Y-12
10. Laboratory Records—RC

EXTERNAL DISTRIBUTION

11. W. H. Casson, LANL, MS-G761, Los Alamos, NM 87545
12. T. Fewell, CDRH/FDA, 5600 Fishers Lane, HFZ MS 143, Rockville, MD 20857
13. T. Heaton, CDRH/FDA, 5600 Fishers lane, HFZ MS 143, Rockville, MD 20857

14-15. C. M. Johnson, NIST, Bld 245, Rm C229, Gaithersburg, MD 20899

16. C. Soares, NIST. Bld 245, Rm C229, Gaithersburg, MD 20899
17. M. N. Varma, Medical Applications and Biophysics Research Division, ER-73, Office of Health and Environmental Research, Department of Energy, 19901 Germantown Road, Germantown, MD 20874-1290

18-19. Office of Scientific and Technical Information, P.O. Box 62, Oak Ridge, TN 37831-0062